ELSEVIER

Journal of Chromatography A, 842 (1999) 229–266

JOURNAL OF CHROMATOGRAPHY A

Review

Non-radioactive electron-capture detector

W.E. Wentworth[a,*], Ju Huang[a], Kefu Sun[a], Yu Zhang[a], Lei Rao[a], Huamin Cai[b], Stanley D. Stearns[b]

[a]*Chemistry Department, University of Houston, Houston, TX 77204-5641, USA*
[b]*Valco Instruments Co., Inc., P.O. Box 55603, Houston, TX 77255, USA*

Abstract

This paper is a review of the research that has been performed on the development and applications of a non-radioactive electron-capture detector (ECD). The ionization in the ECD, normally supplied by a radioactive foil, is supplied by the electromagnetic radiation emanating from a high voltage pulsed discharge in pure helium. This emission consists of a broad band in the vicinity of 13.5–17.5 eV. This is a well know emission arising from a transition in an excited He_2 molecule to a dissociative ground state. The importance of having a high energy process to initiate the ionization in an ECD is emphasized and is the principal reason why the non-radioactive ECD performs in a similar manner to the radioactive ECD. The principal advantage of the non-radioactive ECD is the cleanliness of the detector since the gas chromatography (GC) column effluent does not come in contact with the ionization source. Most radioactive ECDs generally pass the GC column effluent directly over the radioactive foil where the electrons are produced from the emission. Furthermore, the internal volume of the non-radioactive ECD can be made smaller than that of radioactive ECD using ^{63}Ni foils. For this reason, lower make-up gas flow-rates can be used and the sensitivity of the non-radioactive ECD is slightly greater than that for radioactive ECD. The temperature dependence of the non-radioactive ECD closely parallels that of the radioactive detector. This similar behavior is the most definitive criterion that the detectors operate in a similar manner, displaying the different types of electron attachment mechanisms. Applications to the analysis of pesticides, polychlorinated biphenyls and metal complexes have been demonstrated along with their temperature dependence.

Keywords: Reviews; Electron-capture detection; Detection, GC; Detection, LC; Pesticides; Metal complexes; Polychlorinated biphenyls

Contents

*Corresponding author.

0021-9673/99/$ – see front matter
PII: S0021-9673(99)00121-1

1. Introduction

The objective of this paper is to discuss the development, evaluation and status of a non-radioactive electron-capture detector (ECD) that has been commercially available for the past four years. This project was started in late 1989 as a spin-off of a search for a detector for non-chlorinated refrigerating fluids. Several patents related to the detector [1–9] were issued in the period 1992–1996 and research papers describing this work were published shortly afterwards and have continued until the present. In the initial stages of development, PEEK (poly–ether–ether ketone aromatic polymer) and Vespel™ were used as the electrical insulators in the detector and this greatly restricted its performance with regards to the upper operating temperature, due to chemical breakdown or bleeding at $T>175$°C. Subsequent awareness of the machinability and polishing of quartz and sapphire as electrical insulators dramatically improved the performance of the detector at high temperatures. The present version of the detector is quite robust, chemically inert and capable of operating at 400°C in the electron-capture mode.

The initial development of the ECD dates back to 1960 when Lovelock and Lipsky [10] first constructed an ECD which operated at varying bias voltages. Subsequently, it was realized by Lovelock that the maximum capture for many strong electron-capturing compounds occurred at very low electron energies, the lowest of which is the thermal energy distribution with *no* applied bias potential. This was accomplished by applying the bias potential periodically in order to measure the electron concentration. This concept was incorporated into an ECD that was evaluated in a paper by Lovelock and Gregory [11] and the term pulsed electron-capture detector was coined to distinguish it from the use of a variable bias voltage. Most commercial detectors from that time to the present are operated in the pulsed mode. In a later paper, Maggs et al. [12] suggested that the concentration dependence of the detector could be linearized by varying the pulsed frequency. This was justified by a simplified kinetic model but it seems to be effective over a limited range of pulsed frequencies. This concept was also incorporated in most commercial ECDs, since the linearization can be accomplished using simpler electronics. Careful evaluation of the concentration dependence using this technique generally gives linearity over three orders of magnitude, although it is frequently claimed to be higher.

Until the recent development of the non-radioactive ECD, all commercial ECDs utilized a radioactive foil for the generation of electrons by ionization of the make-up gas to the ECD. It would appear from the outside that a radioactive foil is an ideal source of ionization, being a constant, energy-free source with an infinite lifetime. However, this is far from true and it certainly is not energy-free when one considers the effort expended to make the radioactive foil. The radioactive material must be either formed via a nuclear process from an accelerator or concentrated from a naturally occurring source where the concentration of the radioactive material is quite low. Both of these processes are highly energy-dependent so the radioactive foil is not energy-free. Furthermore, the radioactive material must be deposited or adsorbed on the surface of the foil so that the nuclear radiation can escape to ionize the gas above the foil; another process that is not trivial and requires additional energy.

Of course, the nuclear radiation is given off in all directions (360°) and, obviously, only a fraction of the radiation is effective in ionizing the gas above the surface. In other words, there is no control or way to focus the radiation. In addition, there is no control over the range of the nuclear radiation except by the choice of radionuclide. Tritium was one of the first radionuclides used in an ECD and it is a low

energy β-emitter with an average energy of 17.5 keV. Because of this low average energy, the range of tritium β particles is only a few mm in argon. This low range allows for the use of tritium foils in ECDs with low internal volumes, which, in turn, allows the use of lower make-up flow-rates to the detector. This should lead to higher sensitivity since the concentration of the compound is necessarily larger and the ECD response is known to be concentration-dependent and not mass-flow dependent. The principal limitation to the use of tritium foils is its instability at higher temperatures. ^{63}Ni is also a weak β-emitter on a nuclear scale (~2 MeV), but is considerably higher than tritium and the range is consequently much greater. This larger range requires a larger ECD in order to minimize surface ionization from the β particles. The volume of an ECD using ^{63}Ni is typically 0.5–1 ml, requiring flow-rates of 75–150 ml/min in order to retain chromatographic resolution from open tubular, bonded phase fused-silica columns. Recently, a micro ECD was constructed that separates the ionization region from the electron-capture region, which was similar in design to the non-radioactive pulsed discharge (PD) ECD that had been developed earlier. Apparently, the internal volume of the electron-capture region can be reduced in this manner, which should lead to greater sensitivity. The author is not aware of any journal publication describing this detector so no further comparisons with the PDECD can be made at this time.

The radioactive nuclides used in ECDs have long half-lives (^{3}H, 12.32 years; ^{63}Ni, 100 years) [13] and one generally thinks that the radioactive foil has an unlimited lifetime. However, if the ECD is used frequently, the lifetime of the foil is limited by its contamination and subsequent deterioration from repeated samples passing through the detector. This is especially severe for certain compounds that may be reactive towards the metal foil. For example, iodine compounds are quite unstable due to the low energy of the C–I bond and the radioactive foil is especially susceptible to contamination from iodine compounds. After continual exposure to iodine compounds, the radioactive foil in the ECD will become noticeably darkened and the surface structure appears to be weakened. Eventually, the deterioration and/or contamination of the radioactive foil will cause the standing current to diminish and this is usually associated with a decrease in sensitivity. Eventually, the contaminated radioactive foil must be disposed of and this is somewhat costly since disposal of radioactive wastes must satisfy stringent conditions. In practice, the lifetime of the radioactive foil is dependent upon the extent of its use and the nature of the samples to which it is exposed.

The principle advantage of using a radioactive foil in an ECD is the high energy imparted to the ionization process. Generally, ~40 eV are used to form an ion-pair and a β-particle of, say, 1 MeV could cause 25 000 ion-pairs. Of course, there is a distribution of β-particle energies and lower energy betas will not penetrate the make-up gas as far as more energetic β-particles and, consequently, will produce fewer ion-pairs. Since many of the β-particles will have energies of the order of keVs, the 40 eV will be imparted to each ion-pair. Some of the 40 eV energy is imparted in producing excited species, but a very large part (~8 eV) is used to impart a high translational energy to the ion-pair. When the ion-pair consists of an electron and the remaining positive ion of the make-up gas, most of the translational energy is imparted to the free electron. Consequently, the electron becomes separated at a great distance from the positive ion and the electron-positive ion recombination step is inhibited. This is important to the electron-capture process since the attachment of an electron to a molecule is in competition with the electron-positive ion recombination. If the electron-positive ion recombination is exceedingly fast, the competing molecule–electron attachment process will not be extensive and there will be a very weak EC signal. In the design of a non-radioactive ECD, it is essential that the ionization process simulates the ionization from the radioactive foil.

In the radioactive ECD, either nitrogen or argon–methane is generally used as the detector make-up gas. In both of these gases, there are low energy rotational and vibrational modes in addition to the translational modes that are effective in removing the high translational energy imparted to the electron in the ionization process. In the early stages of the development of the ECD, hydrogen and carbon dioxide were used with argon, but they were not as satisfactory as an argon–methane mixture. From an

early study of the electron-capture mechanism, various concentrations of methane were used, ranging up to 20% [14]. It appeared that a small percentage of methane is as effective as a larger percentage. Since the concentration of methane did not seem to be critical, a concentration of 5–10% was selected since that concentration seemed to give the highest standing current. If pure argon is used as the make-up gas, a lower standing current is obtained. The addition of CH_4 increases the standing current by about 30%. Apparently, there are excited states of argon produced by the β-radiation and methane reacts with these metastables to produce ionized species. The methane obviously plays a dual role by: (1) reacting with excited states to give additional ionization; (2) removing translational energy from the electrons to obtain a thermal distribution.

The production and use of radioactive ECDs has extended over the past ~35 years and during this period there have been several attempts at producing a comparable non-radioactive detector. At the very beginning of the commercialization of ECDs, a non-radioactive version was commercialized by Beckman Instruments [15]. It consisted of a separate discharge region in which the ionized species were produced and these were flowed into a reaction zone where the electron-capture processes took place. Difficulties were experienced in maintaining the discharge stable and it was not on the market long. Possibly, some of this instability arose from the column effluent entering the discharge region. The ionization could very well have been photoionization except that, at that time, we did not have the ability to purify the helium sufficiently and the photon emission most likely would have come from impurities such as nitrogen.

A similar approach was taken by Wentworth et al. [16,17] where a microwave source was used to cause ionization/excitation in helium prior to entering the electron-capture region. The detector's performance was similar to that of a radioactive ECD except that the noise in the baseline was considerably higher. Furthermore, the microwave source creates considerable heat and it is difficult to control the temperature in the electron-capture region. In these studies, methane was used as the dopant that can be ionized by the excited species in helium. The methane is also effective in removing the high translational energies of the electron so that it can maintain a thermal distribution. When methane was not used as the dopant, the detector operated as an ionization detector.

In two other studies, surface ionization was used as the source of electrons. The first of these was by Neukermans et al. [18], where the electrons were emitted from a cathode consisting of a platinum wire coated with barium zirconate. A guard gas was passed over the cathode to protect it from contamination by solvents and impurities from the chromatographic system. In the second study by Simmonds [19] the electrons were emitted from a metal surface via the photoelectric effect using ultraviolet radiation. Since the surface was ionized, only free electrons were generated in the gas phase. The detector showed high sensitivity for sulfur hexafluoride but could not be operated at high temperatures.

The problem with both of these studies is that surface ionization creates a negatively charged plasma of electrons, which is inherently less stable due to electronic repulsion than a neutral plasma with both positive ions as well as the negatively charged electrons. Furthermore, the positively charged solid surface has a strong attraction for the gaseous electrons. In order to prevent recombination on the solid surface, the surface could be negatively charged to repel the electrons. It would appear that constructing an ECD using these metal surfaces would require the electron-capturing species to be intimately in contact with the metal surface. For high boiling compounds, this could lead to contamination of the metal surfaces, which, in turn, would lead to instability in the detector.

In order to simulate the initial ionization process that occurs in a radioactive ECD, a pulsed discharge in very pure helium has been used in our laboratory to generate high-energy photons, which are used to photoionize a dopant added downstream of the discharge. Thus the name, pulsed discharge electron-capture detector (PDECD) [20]. The photon emission in helium arises from an excited species of He_2 that has an energy distribution primarily in the range 13.5–17.5 eV [21]. This energy is sufficient to ionize all compounds or elements except for neon. If a dopant is not added downstream, the high energy photons will photoionize the GC eluents and the detector operates as a universal photoionization detector, thus the name, pulsed discharge photoioni-

zation detector (PDPID) [22,23]. It has been shown that when low concentrations of argon or krypton are added to the discharge gas, the resonance lines of Ar and Kr emitted are of lower energy than the emission from helium [24–26]. Thus, photoionization using the Ar- or Kr-doped discharge gives selective photoionization based on the GC eluent having an ionization potential that is less than the energy of the resonance lines of Ar and Kr. In order to distinguish the photoionization from these different discharge sources, we use the symbol of the emitting element as a prefix, thus, He-PDPID, Ar-PDPID and Kr-PDPID.

The reason for using the high energy emission from He_2 in the PDECD is to impart a high translational energy to the electrons so that they will be separated at long distances from the positive ions. It is well known from photoelectron spectroscopy that the energy of the photon in excess over the ionization potential is imparted principally to the lighter dissociative particle, which, in this case, is the electron. This large separation between the electron and positive ion inhibits the recombination and allows more time for the electron attachment process to occur, thus enhancing the sensitivity of the ECD. It is this feature of the PDECD that makes it function in a manner similar to that of the radioactive ECD. The principal difference between the radioactive and nonradioactive ECD is the mode of ionization using a β-particle in the former versus a high energy photon in the latter.

In a much earlier study [27], photoionization was used to generate the electrons for a non-radioactive ECD. However, the photon source was the well known α-Lyman hydrogen emission generated in a microwave cavity. A magnesium fluoride window was used to separate the photon source from the electron-capture region. The transmission of the magnesium fluoride window restricts the photon energy that can be used to $<$10.25–10.3 eV. The α-Lyman hydrogen at 10.2 eV is about the highest energy photon that will be transmitted through magnesium fluoride. With this low energy photon source, the non-radioactive ECD did not have sensitivities comparable to those of the radioactive ECD. Similarly, Kapila et al. [28] constructed a photoionization ECD using a rare gas resonance lamp (HNU Systems), which also uses a magnesium fluoride window. In both studies, the dopant used was tri-*n*-propylamine, which has an offensive odor and cannot be vented into a laboratory or plant. The present configuration of the non-radioactive ECD differs from these in that the photoionization of the dopant occurs without a window, thus allowing the use of any radiation that is transparent in helium.

2. Experimental

During the developmental stage of the non-radioactive ECD, slightly different configurations of the detector were used. At this time, we will describe only the most recent, commercially available detector. Deviations in detectors used in previous studies will be pointed out if they affect the results of that study. A schematic diagram of the PDECD is shown in Fig. 1. The dopant is introduced between the upper two electrodes where there is a slight difference in potentials, to assist the migration of the electrons into the electron-capture region between the two lower electrodes. The GC column is introduced to the detector through a fitting at the bottom and its position is adjusted so that the effluent from the column enters at the middle electrode in the upper portion of the electron-capturing region. Sapphire insulators are used to separate the bias electrodes and the collector electrode. Helium discharge gas is introduced at the top of the detector and flows through the discharge and into the ionization region. A flow-rate of 30–40 ml/min of helium is sufficient to prevent diffusion of the dopant into the discharge region. The high energy photons from the discharge pass through the helium into the ionization region where the dopant is introduced.

Since this is a review article, information from different studies will be included. For this reason, it would be inappropriate to delineate the experimental conditions for each of these studies. The reader will have to consult the original papers for the details. The gas chromatographic conditions will be stated where it is essential.

In all of these studies, the helium used was either five-nines (99.999% pure) or six-nines (99.9999% pure) and it was further purified by passing it through a Valco helium purifier operated at 400°C. A helium purifier is supplied with the detector as well

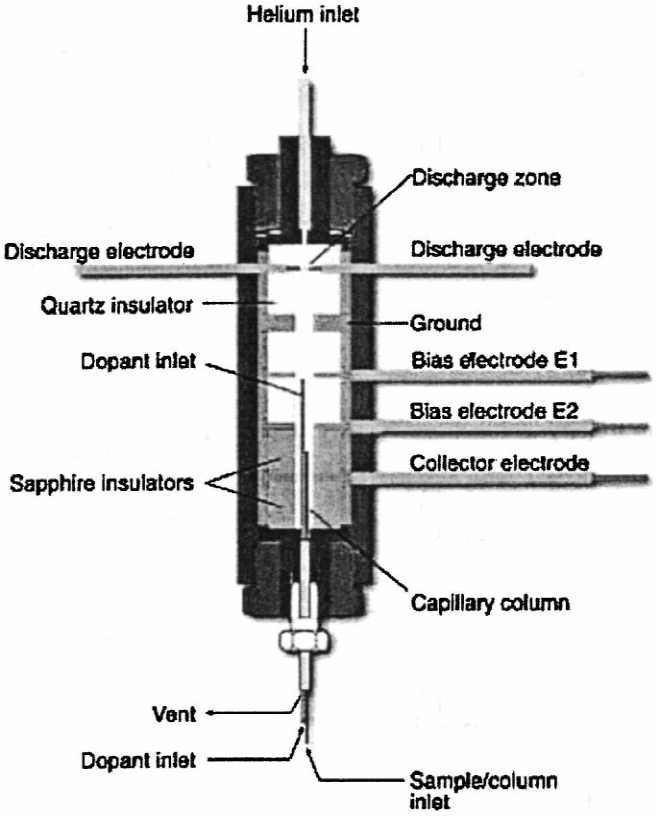

Fig. 1. Schematic diagram of PDECD.

as a fixed restrictor so that the helium flow into the discharge section of the detector can be regulated by adjusting the pressure at the helium cylinder. It is essential that this direct connection from the helium supply to the detector be used. *Do not* use flow controllers etc., which are frequently supplied with the gas chromatograph, since they generally do not have sufficiently leak-free connections and the flow controllers frequently are sources of moisture, if not leaks, and this is very detrimental to the performance of the detector. All the lines leading to the purifier and the fixed restrictor are cleaned meticulously by the manufacturer and capped with end fittings to prevent contamination.

If an alternate helium supply is required to satisfy factory or laboratory regulations, extreme care must be exercised to ensure that it retains at least five-nines purity prior to passing it through the helium purifier. Under all circumstances, avoid the use of copper tubing and brass fittings.

As the detector is in use, the standing current in the He-PDPID mode should be monitored weekly. If a rise in the standing current is observed, it is likely that the getter material in the purifier is nearly spent and should be replaced. Instructions are provided which describe the replacement procedure.

3. Kinetic model

3.1. Kinetic model

The pulsed discharge is generally operated at a frequency of ~3.3 kHz or an interval of ~300 μs. The discharge appears to be more stable at this frequency and a relatively high standing current is

obtained compared to the radioactive ECD. In the ECD mode, a low bias voltage is applied for the collection of electrons. A voltage of 1–5 V on the center electrode will give a standing current of 10–50 nA. The commercial detector has a fixed bias voltage of 2.5 V on the center electrode and this is satisfactory when methane (~0.3%) is used as the dopant. With this small voltage and relatively high pressure (1 atm; 1 atm=101 325 Pa), the energy distribution of the electrons should be close to thermal. For many compounds, the maximum electron attachment cross section occurs at near zero energy and, for this reason, most ECDs operate at low electron energies. In the radioactive detector, this is accomplished by allowing the electron attachment reaction to occur at zero field between the pulsed bias voltages.

Even though the discharge is pulsed in the PDECD, we can consider the photoionization to be continuous in the time frame of the ECD responses, which is of the order of 10 Hz. With this assumption, the kinetic analysis of the reactions in the PDECD can be carried out in a manner similar to that for the radioactive ECD [29,30]. Since the extent of ionization in the PDECD depends on the time-averaged intensity of the photon source from the discharge, we will designate the rate of production by $k_P\ I\ [D]$ where '*I*' refers to the intensity of the photon source and k_P is the rate constant. k_P will include the absorption coefficient and the photoionization efficiency of the dopant, D. The reaction steps in the general kinetic mechanism, assuming only one electronic state for the negative ion, are given by

$$h\nu + D \xrightarrow{k_P I} D^+ + e^- \quad (1)$$

$$e^- + D^+ \xrightarrow{k_D} D \quad (2)$$

$$e^- + AB \xrightarrow{k_1} AB^- \quad (3)$$

$$AB^- \xrightarrow{k_{-1}} AB + e^- \quad (4)$$

$$AB^- \xrightarrow{k_2} A + B^- \quad (5)$$

$$AB^- + D^+ \xrightarrow{k_{N_1}} AB + D \quad (6)$$

$$B^- + D^+ \xrightarrow{k_{N_2}} B + D \quad (7)$$

$$e^- \xrightarrow{\mu\nu/A} \text{electrometer} \quad (8)$$

The last reaction step, Eq. (8), is added to represent the continuous removal of electrons by application of a low potential of a few volts. This step differs from the kinetic analysis of the radioactive ECD where the electrons are collected by applying a pulsed potential at low frequencies. The symbol, μ, represents the mobility of the electron ($cm^2\ s^{-1}\ V^{-1}$), A is the cross-sectional area of the detector (cm^2), and ν is the applied potential over the last pair of electrodes. Since we do not have parallel plate electrodes, it is difficult to define the cross-sectional area, A. However, $\mu\nu$ is divided by A to give the proper units of s^{-1}.

When there is no capturing species present, $[AB]=0$, only reaction steps (1) and (2) are involved and the rate expression for $[e^-]$ production is

$$\frac{d[e^-]}{dt} = k_P\, I[D] - k_D[D^+]\,[e^-] - (\mu\nu/A)[e^-] \quad (9)$$

Assuming steady state and letting $[e^-]=b$ when $[AB]=0$

$$0 = k_P I[D] - (k_D[D^+] + \mu\nu/A)b$$

or

$$b = \frac{k_P I[D]}{(k_D[D^+] + \mu\nu/A)} \quad (10)$$

The concentration '*b*' is related to the standing current, which we will consider later.

When the capturing species AB is present, rate expressions for e^-, AB^- and B^- can be written based upon the mechanism in reaction steps (1)–(8). In the previous kinetic analysis of the mechanism for the radioactive ECD, it was assumed that the concentration of AB was far in excess of that for e^- and that $[AB]=[AB]^0$ = initial concentration of AB. This was justified by the relatively small standing current for the radioactive ECD (~2–4 nA). Typically, the non-radioactive ECD has a higher standing current and the concentration of e^- can be as large as that for AB. Consequently, we include a mass balance for AB in the analysis.

The rate expressions for the reaction steps (1)–(8) and the mass balance are given as follows:

$$\frac{d[e^-]}{dt} = k_P I[D] - k_D[D^+][e^-] - (\mu\nu/A)[e^-] - k_1[AB][e^-] + k_{-1}[AB^-] \quad (11)$$

$$\frac{d[AB^-]}{dt} = k_1[AB][e^-] - k_{-1}[AB^-] - k_2[AB^-] - k_{N_1}[D^+][AB^-] \quad (12)$$

$$\frac{d[B^-]}{dt} = k_2[AB^-] - k_{N_2}[D^+][B^-] \quad (13)$$

$$[AB]^0 = [AB] + [AB^-] + [B^-] \quad (14)$$

If we assume steady state in Eqs. (11)–(13), [AB], $[AB^-]$ and $[B^-]$ can be eliminated from Eqs. (11)–(13), leaving a relationship between $[e^-]$ and $[AB]^0$. Eq. (13) can be solved for $[B^-]$

$$\frac{d[B^-]}{dt} = 0 = k_2[AB^-] - k_{N_2}[D^+][B^-]$$

$$[B^-] = \frac{k_2[AB^-]}{k_{N_2}[D^+]} \quad (15)$$

Eq. (12) at steady state can be solved for [AB] in terms of $[AB^-]$

$$[AB] = \frac{k_{-1}[AB^-] + k_2[AB^-] + k_{N_1}[D^+][AB^-]}{k_1[e^-]} \quad (16)$$

Substituting Eqs. (15) and (16) into Eq. (14)

$$[AB]^0 = \frac{k_{-1}[AB^-] + k_2[AB^-] + k_{N_1}[D^+][AB^-]}{k_1[e^-]} + [AB^-] + \frac{k_2[AB^-]}{k_{N_2}[D^+]}$$

Solving for $[AB^-]$

$$[AB^-] = \frac{[AB]^0}{\frac{k_{-1} + k_2 + k_{N_1}[D^+]}{k_1[e^-]} + 1 + \frac{k_2}{k_{N_2}[D^+]}} \quad (17)$$

Eqs. (11) and (12) at steady state can be added to eliminate [AB]

$$0 = k_P I[D] - k_D[D^+][e^-] - (\mu\nu/A)[e^-] - k_2[AB^-] - k_{N_1}[D^+][AB^-] \quad (18)$$

Rearranging Eq. (18) and substitution for $[AB^-]$ from Eq. (17)

$$k_P I[D] - (k_D[D^+] + \mu\nu/A)[e^-] = \frac{(k_2 + k_{N_1}[D^+])[AB]^\circ}{\frac{k_{-1} + k_2 + k_{N_1}[D^+]}{k_1[e^-]} + 1 + \frac{k_2}{k_{N_2}[D^+]}}$$

Dividing by $(k_D[D^+] + \mu\nu/A)$, substituting for '*b*' from Eq. (10), and simplifying

$$b - [e^-] = \frac{k_2 + k_{N_1}[D^+]}{(k_D[D^+] + \mu\nu/A)} \times \frac{k_1[e^-]k_{N_2}[D^+][AB]^\circ}{k_{N_2}[D^+](k_{-1} + k_2 + k_{N_1}[D^+]) + k_1[e^-]k_{N_2}[D^+] + k_2k_1[e^-]}$$

$$\frac{b - [e^-]}{[e^-]} k_{N_2}[D^+](k_{-1} + k_2 + k_{N_1}[D^+]) + (b - [e^-]) \times (k_1k_{N_2}[D^+] + k_1k_2) = \frac{k_{N_1}[D^+] + k_2}{(k_D[D^+] + \mu\nu/A)} k_1k_{N_2}[D^+][AB]^0$$

$$\frac{b - [e^-]}{[e^-]} + (b - [e^-]) \frac{k_1(k_{N_2}[D^+] + k_2)}{k_{N_2}[D^+](k_{-1} + k_2 + k_{N_1}[D^+])} = \frac{(k_{N_1}[D^+] + k_2)}{(k_D[D^+] + \mu\nu/A)} \frac{k_1}{(k_{-1} + k_2 + k_{N_1}[D^+])} [AB]^0 \quad (19)$$

In Eq. (19), the $[e^-]$ and '*b*' represent the concentration of electrons with and without the presence of the electron-capturing species, AB. These cannot be measured directly, but by the application of a small potential, a small fraction of these are continuously collected and recorded as a current by the electrometer. This current is directly proportional to the concentration of electrons present, as represented by the reaction step in Eq. (8).

$$I_{e^-} = \frac{\mu\nu}{A} V\ 96\ 500\ [e^-] \quad (20)$$

where the Faraday = 96 500 C/equivalent has been included for the conversion to coulombs, V = volume of the detector in liters, and the current, I_{e^-}, will be in Amps. We will have an analogous expression for the standing current of the detector when AB is not present

$$I_b = \frac{\mu\nu}{A} V\ 96\ 500\ b \quad (21)$$

Solving for $[e^-]$ and b from Eqs. (20) and (21), respectively, and substitution into Eq. (19) gives

$$\frac{I_b - I_{e^-}}{I_{e^-}} + \frac{(I_b - I_{e^-})}{\frac{96\,500\,\mu\nu}{A}V} \frac{k_1(k_{N_2}[D^+] + k_2)}{k_{N_2}[D^+](k_{-1} + k_2 + k_{N_1}[D^+])} = \frac{(k_{N_1}[D^+] + k_2)}{(k_D[D^+] + \mu\nu/A)} \frac{k_1}{(k_{-1} + k_2 + k_{N_1}[D^+])} [AB]^0 \quad (22)$$

In Eq. (22), there are two terms on the left side of the equation, the first of which occurs when [AB] is assumed to be in excess of '*b*' so that $[AB] \sim [AB]^0$. This is the expression arrived at for the radioactive ECD and is appropriate also for the non-radioactive ECD. If this term is dominant over the second term, Eq. (22) becomes

$$\frac{I_b - I_{e^-}}{I_{e^-}} = \frac{k_1}{(k_D[D^+] + \mu\nu/A)} \frac{(k_{N_1}[D^+] + k_2)}{(k_{-1} + k_2 + k_{N_1}[D^+])} [AB]^0 = K[AB]^0 \quad (23)$$

where K = electron-capture coefficient. Note that the response, $(I_b - I_{e^-})/I_{e^-}$, is independent of ν if $k_D[D^+] >> \mu\nu/A$; i.e. at low voltages, the expression is the same as in the radioactive ECD. However, at higher voltages $\mu\nu/A >> k_D[D^+]$, the response is inversely proportional to ν and will be decreased as ν is increased.

The second term on the left side of Eq. (22) occurs when '*b*' is in excess of $[AB]^0$ and has the form expected from a Coulometric response for the ECD. If the second term on the left side of Eq. (22) is dominant, then Eq. (22) becomes

$$(I_b - I_{e^-}) = 96\,500 \frac{\mu\nu}{A} V \times \frac{(k_{N_1}[D^+] + k_2)}{k_{N_2}[D^+] + k_2)} \frac{k_{N_2}[D^+]}{(k_D[D^+] + \mu\nu/A)} [AB]^0 \quad (24)$$

Generally, k_{N_1} and k_{N_2} are similar in magnitude regardless of the ions involved since they are highly exothermic charge neutralization steps. Consequently, Eq. (24) would be similar for all compounds, a result that you would expect from a coulometric response. However, in order for a compound to give a coulometric response, it must be an exceedingly strong electron-capturer, such as CCl_4. The reason for this is simply that, for strong electron-capturers, the concentration will necessarily be low, making the requirement $[AB]^0 << b$ more plausible. For moderate to weak capturing compounds, Eq. (24) will never be realized. For strong electron-capturers, there will be a transition of the dominance of the terms on the left side of Eq. (22) as the concentration is increased. Note in Eq. (24) that the signal is proportional to ν if $k_D[D^+] >> \mu\nu/A$, but becomes independent of ν when $\mu\nu/A >> k_D[D^+]$.

3.2. Dopant for ionization/thermalization

It is difficult to discuss one aspect of the non-radioactive ECD without involving other parameters. However, for the sake of simplicity, we will attempt to discuss each separately and include other factors only when necessary. In the non-radioactive ECD, it is necessary to introduce a dopant that can be photoionized by the He_2 emission from the discharge and will produce the necessary standing current for the electron-capture mode. Since the He_2 emission can ionize all substances except neon, it would appear that any substance could be used as the dopant. There is considerable latitude in selecting a dopant, but there are additional requirements that restrict the selection. In order to be compatible with the electron-capture process, first the dopant must be relatively inert to electron capture, i.e., it should have an electron affinity of essentially zero. Secondly, it would be preferable that the dopant have a low ionization potential so that there will be more excess energy in the photoionization that can be imparted to the electron, thus reducing the rate of electron-positive ion recombination. Thirdly, the dopant should have internal rotational and vibrational modes that can be used to reduce the high translational energy of the electron to a thermal distribution.

Several substances have been investigated for possible use as the dopant in the PDECD. In Table 1, we list possible dopants along with their ionization potentials. Some of these have been investigated in previous studies and others are potential candidates that are currently being considered. Table 1 lists the

Table 1
Possible dopant compounds

Compounds	Formula	Ionization potential (eV)
Hydrogen	H_2	15.43
Nitrogen	N_2	15.58
Carbon dioxide	CO_2	13.77
Methane	CH_4	12.6
Xenon	Xe	12.21
Ethane	C_2H_6	11.5
Propane	C_3H_8	11.1
n-Butane	C_4H_{10}	10.63
Ethylene	C_2H_4	10.5
Ammonia	NH_3	10.2
Hexane	C_6H_{14}	10.18
Heptane	C_7H_{16}	9.90
2,2,4-Trimethylpentane (isooctane)	C_8H_{18}	9.86
Propene	C_3H_6	9.73
1-Butene	1-C_4H_8	9.6
Benzene	C_6H_6	9.24
Toluene	$C_6H_5CH_3$	8.82

potential dopants in order of decreasing ionization potential. In the initial study of the development of the PDECD [20], the following compounds were considered as dopants: H_2, N_2, CO_2, CH_4 and NH_3. These were evaluated using relatively volatile chlorinated compounds. Since these compounds most certainly undergo dissociative electron-capture, the role of the dopant in terms of thermalization of the electron energy is probably less important. Nevertheless, the capture coefficients were evaluated for four compounds and compared with that for the radioactive ECD. In general, the capture coefficients using N_2, H_2, CO_2 and NH_3 as dopants gave electron-capture coefficients of the order of, or in excess of, those for the radioactive ECD. The capture coefficients using $CO_2$and NH_3 are slightly greater than those with N_2 and H_2; however, the baseline was noisier with CO_2 and NH_3. In this initial investigation, the sample plus make-up gas were passed through the discharge and the additional dopant could certainly affect the stability of the baseline. Later in this initial study [20], only the helium make-up gas was passed through the discharge, in the same manner as described earlier in Section 2 and this configuration greatly improves the stability of the baseline. The use of CH_4as dopant was investigated in this configuration and found to give less disturbance when the solvent (2,2,4-trimethylpentane) is eluted compared to the use of H_2 as dopant. Since H_2 and N_2 have higher ionization potentials than CH_4, one would expect solvents with much lower ionization potentials to increase the standing current and this effect is diminished with CH_4. On the basis of this study [20], the use of H_2 or N_2 as dopant gas appears to be satisfactory for dissociative electron capture, including the analysis of pesticides.

However, the electron capture to compounds that form stable negative ions rather than dissociative capture are more discerning of the dopant used. In a later study [31], a large variety of compounds were studied using the PDECD at 100°C and these included some compounds that formed stable negative ions. When hydrogen was used as the dopant, there was reasonable agreement between the electron-capture coefficients for the PDECD and the radioactive ECD for 12 out of a total of 16 compounds. For these 12 compounds, the ratio of the electron-capture coefficient for the PDECD to that for the radioactive ECD ranged from 0.1 to 4.1, with an average of 0.38. The four compounds with a ratio outside this range are acetophenone (0.003), benzaldehyde (0.005), chlorobenzene (0.0) and iodobutane (100). Acetophenone and benzaldehyde are only moderately strong electron-capturers and their response in the PDECD is exceedingly small when H_2 is used as the dopant. Chlorobenzene is a very weak electron-capturing compound, especially at lower temperatures. However, it is detectable with a radioactive ECD, whereas no signal was observed with the PDECD using H_2 as dopant. On the other hand, iodobutane has an exceptionally high electron-capture coefficient using H_2 as the dopant, much higher than that observed with the radioactive ECD. Apparently, a slightly higher electron energy in H_2 more closely matches the electron attachment cross section for iodobutane and there is a significantly greater electron-capture coefficient. In a more recent study [32], extra care was exercised in drying the H_2 dopant and the dry H_2 dopant was found to be less satisfactory. Apparently, traces of moisture in previous studies assisted the effectiveness of H_2 as a dopant.

Methane was also considered as the dopant for the electron capture of 24 chloro compounds, 14 bromo compounds, and iodomethane [31]. For the com-

pounds that were previously studied with the radioactive ECD, the ratio of electron-capture coefficients ranged from 0.3 to 3.0, with two exceptions: chlorobenzene 20 and iodomethane 100. The average ratio for the compounds in the range of 0.3 to 3.0 was 1.8 for 19 compounds. Obviously, the use of methane as the dopant in the PDECD more closely parallels and is slightly more sensitive than the radioactive ECD.

In a more recent study, the electron-capture coefficients for acetophenone and benzaldehyde were obtained with the PDECD using methane as the dopant [33]. The values were very close to those obtained from a radioactive ECD and even more significant is the fact that the temperature dependence of the electron-capture coefficient for acetophenone and benzophenone closely agrees with the radioactive ECD result. If a thermal distribution were not obtained, the temperature dependence would show the greatest difference since the temperature dependence is based solely on the thermal energy distribution of the electron, the molecule AB, and the molecular ion AB^-. For this reason, we conclude that using CH_4 as the dopant in the PDECD gives a thermal distribution of energies and is preferable over H_2 and N_2 as dopants. This is not too surprising if one considers the fact that CH_4 has 15 internal modes compared to a diatomic molecule with only six. Probably most important are the low energy bending vibrational modes in CH_4 that would be most effective in removing excess energy imparted to the electron upon photoionization. On the other hand, the single vibrational mode in H_2 and N_2 is of very high energy and probably is somewhat ineffective at removing the lower thermal energies of the electron. The results of the temperature dependence will be presented later in this review paper.

CO_2 and NH_3 have not been evaluated as extensively as H_2, N_2 and CH_4, but probably are also more effective dopants than H_2 or N_2. NH_3 would certainly be expected to be as effective if not more effective than CH_4 since it also has low energy bending vibrational modes and a lower ionization potential than CH_4. However, its odor would be objectionable and the effluent would have to be absorbed or incinerated. CO_2 has only two low energy bending modes and its critical point of 31°C must be considered in making high pressure blends. For these reasons, we consider CH_4 to be the best choice and the results of the PDECD using CH_4 closely parallel those of the radioactive ECD.

Xenon has been used as the dopant gas and, for compounds that undergo dissociative electron capture, it is as effective or better than methane [32]. Twenty-three compounds were studied on the PDECD with CH_4, N_2 and Xe as dopants. The electron-capture coefficients for all three dopants were comparable, with the exception of five weakly capturing compounds in which the N_2 dopant gave bipolar or W-shaped peaks. For all compounds, the results with Xe and CH_4 dopants gave closely parallel results, with the values using Xe in slight excess over those with CH_4. All of these 23 compounds were chloro- or bromo-containing, which most certainly undergo dissociative electron capture, so the good agreement is not surprising. In a more recent study [34], acetophenone and benzaldehyde were run on the PDECD using Xe as dopant and the results differed from those using the radioactive ECD but the difference was not as great as those found in the previous study with H_2 [31]. It would appear that Xe is a more efficient dopant than N_2 or H_2 but not as good as CH_4. Since Xe has only translational degrees of freedom, one may be surprised that Xe is an effective dopant. However, Xe has a large atomic number (54) and with this many electrons, the atoms are easily polarizable. It is very likely that the small, charged electron has very strong ion-induced dipole interactions with Xe. The lower ionization potential of xenon also will be beneficial in reducing the electron-positive ion recombination. An advantage of using Xe as dopant is that its possible diffusion into the discharge region will not cause contamination of the electrodes like a carbon-containing dopant. Another advantage is that the PDECD using Xe could be connected in series with a flame ionization detector (FID) without any increase in background. In fact, the PDECD would supply the necessary make-up gas to the FID.

Other potential dopants which have more complicated structures are shown in Table 1. Obviously, they would have many internal modes of motion and should be effective at removing the excess energy of the electron. These molecules should have several electrons that can be photoionized with the He_2 emission and, potentially, the use of these molecules

as dopants could give a higher standing current. Some of these will be discussed near the end of this paper.

3.3. Concentration dependence

It is well known from experimental data that the response to a radioactive ECD is not linear with concentration except at very low percent capture, say less than 1–2%. If measurements were restricted to this low range, the dynamic range of the ECD would be very limited and the detector would not be very practical. The same situation exists for the non-radioactive ECD since it closely mimics the radioactive version.

There is one major difference between the radioactive and the non-radioactive ECD and this is in the magnitude of the standing current. The radioactive ECD has a somewhat fixed limitation in that the level of radioactivity should be adequate to operate the ECD but not be so excessive as to make it unsafe. Standing currents can change considerably due to cleanliness of the detector, but values of 3–5 nA are considered to be quite satisfactory. With the non-radioactive ECD, we do not have these safety restrictions and the standing current can be varied considerably by varying the intensity of the pulsed discharge source. The intensity of the pulsed discharge depends upon two factors: (1) the amount of charge supplied to each pulse, which is controlled by the voltage applied for a regulated time (pulse width) and (2) the frequency of the pulsed discharge. Standing currents as high as 50 nA can be obtained and one is tempted to use a high standing current since it can generally be measured more precisely. However, one must also consider the effect that the standing current has on the electron-capture process and this is very detrimental at high standing currents. The reason for this was revealed in the kinetic model and the development of Eq. (22). As mentioned previously, the second term on the left side is dominant when '*b*', the concentration of electrons with $[AB]=0$, is large. A large '*b*' value can be related directly to a high standing current, I_b, as was shown previously by Eq. (21).

The commercial detector described in Fig. 1 contains an electronic package that not only supplies the pulsed voltage for the discharge, but also a microprocessor that calculates $(I_b-I_{e^-})/I_{e^-}$ from the observed I_b and I_{e^-}. I_b is set by depressing the reset button prior to the elution of the GC peak and is assumed to be constant through the peak. The linearized signal can be fed directly into the GC software where integration of GC peaks can be performed. This analysis has been carried out for CCl_4, $CHCl_3$, CH_2Cl_2 and C_2Cl_4 [32]. When an integration is performed, the integral of $(I_b-I_{e^-})/I_{e^-}$ over the peak is related to the moles of AB (n_{AB}) passing through the detector by

$$\text{Peak area} = \int \frac{I_b - I_{e^-}}{I_{e^-}} \frac{dV}{dt}\, dt = K\, n_{AB} \tag{25}$$

where dV/dt is the flow-rate through the detector. In order to evaluate the linear dynamic range of the PDECD over a large range of concentrations, the logarithm of the integral on the left side of Eq. (25) is plotted versus the logarithm of n_{AB}, and one expects a linear graph with a slope of one. This has been done in Fig. 2 for the compounds CCl_4, $CHCl_3$ and C_2Cl_4. For CCl_4, the linear relationship is obeyed up to ~60 pg. Since the MDQ (minimum detectable quantity) for CCl_4 is 6 fg = 0.006 pg, the linear dynamic range is 10^4. For the other compounds, the linear relationship is obeyed up to a higher mass, but the MDQ is correspondingly larger and the linear dynamic range is similar to that for CCl_4.

An alternative mode of linearization of the PDECD signal is to vary the bias voltage (V) in order to maintain a constant current [35]. This is abbreviated as the cc-mode (constant current) in contrast to the constant potential (cp-mode). The rationale for the cc-mode is based upon the $(I_b-I_{e^-})/I_{e^-}$ in Eq. (19). Previously in Eqs. (20) and (21), we gave the relationship between the current, concentration of electrons, bias voltage, mobility of the electron and constants. The standing current of the detector is now given by

$$I_b = \frac{\mu \nu_b}{A} V\ 96\ 500\ b = C \nu_b b \tag{26}$$

where ν_b is the bias voltage used to obtain this standing current and $C=(\mu/A)\ V\ 96\ 500=\text{constant}$.

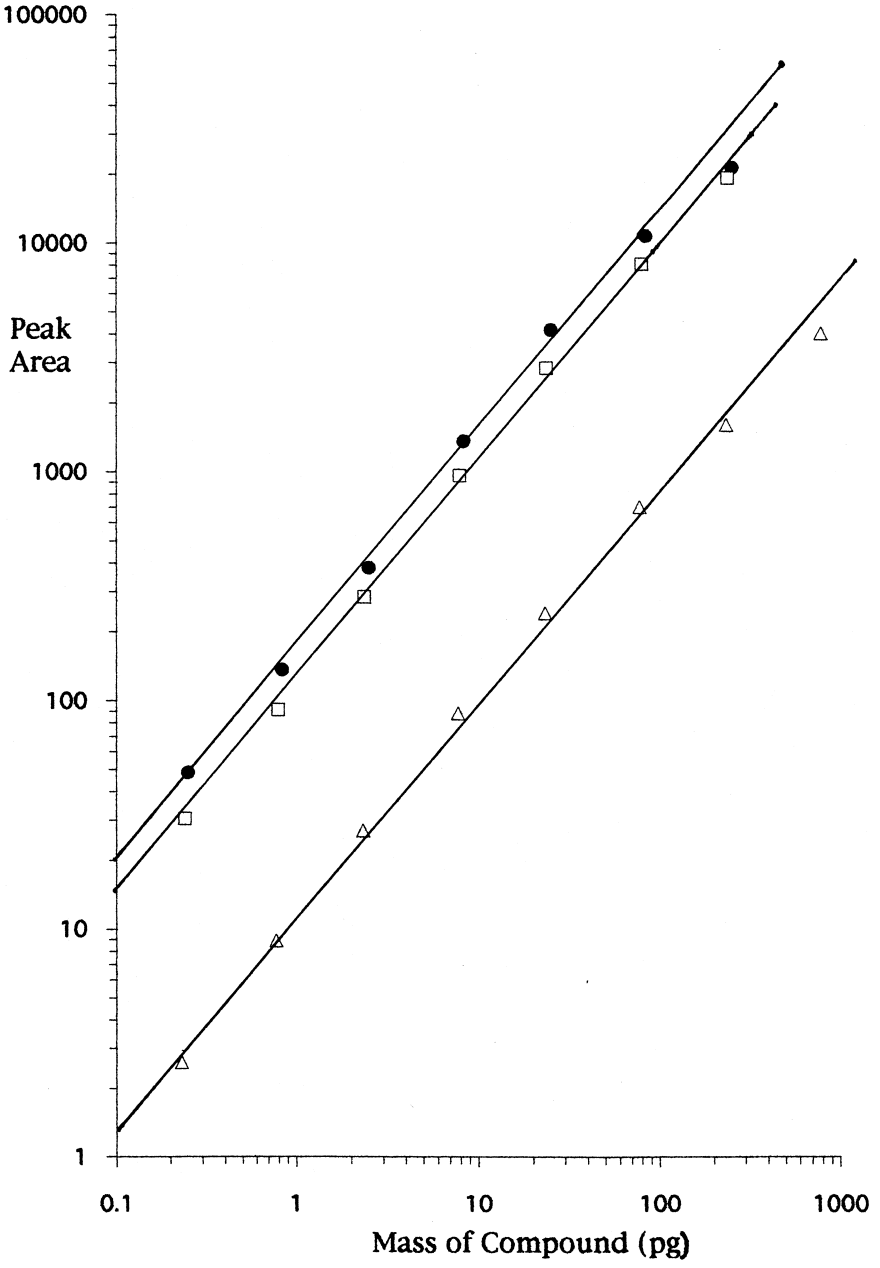

Fig. 2. Concentration dependence of CCl_4 in the constant potential mode $\nu_1 = -20$ V, $\nu_2 = -0.75$ V.

When the capturing compound, AB, is present, the current is given by I_{e^-}, however, in the cc-mode, the bias voltage, ν_{e^-}, is increased in order to make $I_{e^-} = I_b$. Thus,

$$I_b = \frac{\mu \nu_{e^-}}{A} V\ 96\ 500\ [e^-] = C\nu_{e^-}[e^-] \quad (27)$$

We now solve for b and $[e^-]$ from Eqs. (26) and

(27) and substitute into Eq. (19). The term $(b-[e^-])/[e^-]$ would become

$$\frac{b-[e^-]}{[e^-]} = \frac{\dfrac{I_b}{C\nu_b} - \dfrac{I_b}{C\nu_{e^-}}}{\dfrac{I_b}{C\nu_{e^-}}} = \frac{\dfrac{1}{\nu_b} - \dfrac{1}{\nu_{e^-}}}{\dfrac{1}{\nu_{e^-}}} = \frac{\nu_{e^-}}{\nu_b} - 1$$

$$= \frac{\nu_{e^-} - V_b}{\nu_b} \tag{28}$$

The term $(b-[e^-])$ would become

$$(b-[e^-]) = \frac{I_b}{C\nu_b} - \frac{I_b}{C\nu_{e^-}} = \frac{I_b}{C}\left(\frac{1}{\nu_b} - \frac{1}{\nu_{e^-}}\right)$$

$$= \frac{I_b}{C}\frac{\nu_{e^-} - \nu_b}{\nu_b\nu_{e^-}} = b\nu_b\left(\frac{\nu_{e^-} - \nu_b}{\nu_b\nu_{e^-}}\right)$$

$$(b-[e^-]) = b\frac{\nu_{e^-} - \nu_b}{\nu_{e^-}}$$

$$= \frac{k_P I[D]}{k_D[D^+] + \mu\nu/A}\frac{\nu_{e^-} - \nu_b}{\nu_{e^-}} \tag{29}$$

Substituting Eqs. (28) and (29) into Equation (19) gives the general expression in the cc-mode, which is comparable to Eq. (22) in the cp-mode.

$$\frac{\nu_{e^-} - \nu_b}{\nu_b} + \frac{k_P I[D]}{k_D[D^+] + \mu\nu/A}\frac{\nu_{e^-} - \nu_b}{\nu_{e^-}} \times \frac{k_1(k_{N_2}[D^+] + k_2)}{k_{N_2}[D^+(k_{-1} + k_2 + k_{N_1}[D^+])}$$

$$= \frac{(k_{N_1}[D^+] + k_2)}{(k_D[D^+] + \mu\nu/A)}\frac{k_1}{(k_{-1} + k_2 + k_{N_1}[D^+])}[AB]^0 \tag{30}$$

As before, if the first term on the left is dominant, then Eq. (30) becomes

$$\frac{\nu_{e^-} - \nu_b}{\nu_b}$$

$$= \frac{k_1}{(k_D[D^+] + \mu\nu/A)}\frac{(k_{N_1}[D^+] + k_2)}{(k_{-1} + k_2 + k_{N_1}[D^+])}[AB]^0$$

$$= K[AB]^0 \tag{31}$$

If the second term on the left side of Eq. (30) is dominant, then Eq. (30) becomes

$$\frac{k_P I[D]}{k_D[D^+] + \mu\nu/A}\frac{\nu_{e^-} - \nu_b}{\nu_{e^-}}$$

$$= \frac{(k_{N_1}[D^+] + k_2)}{(k_{N_2}[D^+] + k_2)}\frac{k_{N_2}[D^+]}{k_D[D^+] + \mu\nu/A}[AB]^0$$

$$\frac{\nu_{e^-} - \nu_b}{\nu_{e^-}} = \frac{(k_{N_1}[D^+] + k_2)}{(k_{N_2}[D^+] + k_2)}\frac{k_{N_2}[D^+]}{k_P I[D]}[AB]^0 \tag{32}$$

Eq. (31) in the cc-mode is analogous to Eq. (23) in the cp-mode, where K is again the electron-capture coefficient. Since I_b = constant, the linearized function is now simply the difference in the bias voltage required to keep the current constant.

The constant current is maintained through a feedback circuit to adjust the bias voltage. The electronic circuitry for the cc-mode is much simpler than the micro-processor required for the cp-mode. Furthermore, the cc-mode allows linearization to higher concentrations of analyte, increasing the linear range to five orders of magnitude for CCl_4, from 2 fg to 200 pg. This is shown in Fig. 3 where the linear range is evaluated from the region in which the log (integrated response for CCl_4) is linear with the log (mass of CCl_4) with a slope of one. This linear relationship is shown in Fig. 3 for $I_b = 10$ and 20 nA. The range of linearity is about the same for both 10 and 20 nA. The response for 20 nA breaks over at a lower concentration than for 10 nA, however, the lower limit is also lowered and the range is about the same as that for $I_b = 10$ nA.

Even though the same kinetic model applies to both the cp-mode and the cc-mode, there is a difference in that the increased voltage in the cc-mode to compensate for the decrease in $[e^-]$ changes the thermal distribution of the electrons. This will not be significant unless the $[e^-]$ is diminished greatly and a high voltage will be required to maintain a constant current. This effect will be less severe if a low standing current is selected, which will require lower voltages.

Another difference that may arise between the cc-mode and the cp-mode is the effect that a higher voltage would have on the positive ion concentration. In both Eqs. (23) and (31), one may note the presence of the $[D^+]$. Since the electron mobility is far in excess of the mobility of the large positive ion,

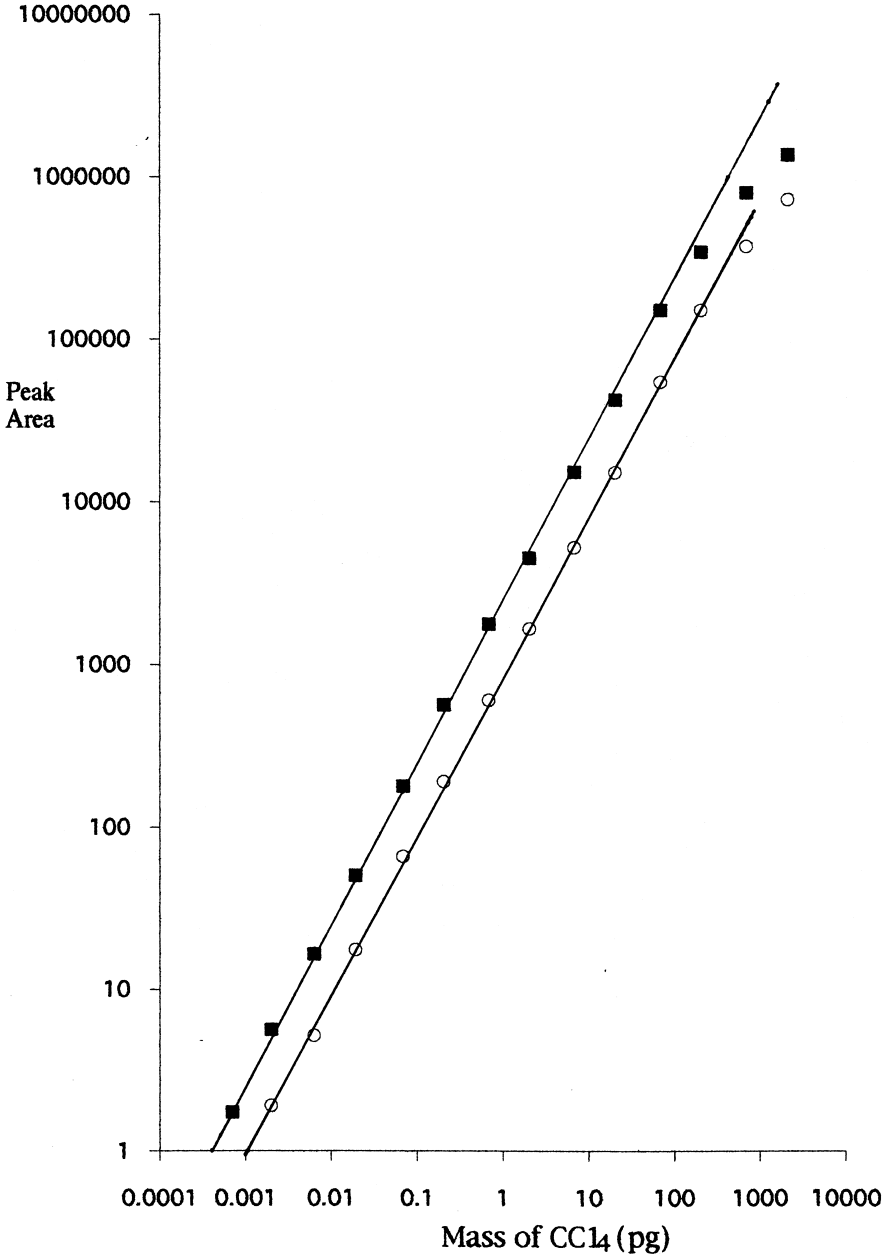

Fig. 3. Concentration dependence of CCl_4 in the constant current mode. $I_b = 10$ nA (○), $I_b = 20$ nA (■).

we expect the $[D^+]$ to remain essentially constant in the presence of a low voltage required to collect the e^-. This should be true in the cp-mode where the voltage is low and remains constant. However, when a highly capturing GC peak is eluted, the bias voltage in the cc-mode must be increased considerably in order to maintain the current constant. This higher voltage may be sufficient to increase the collection of positive ions and $[D^+]$ may decrease. This is probably a minimal effect if the constant current selected is low and the required voltage to maintain this low current will also be low. Also, the

elution of the GC peak is of a short duration when using highly efficient capillary columns, and the large build-up of $[D^+]$ during the application of a low voltage between peaks will probably not be disturbed significantly during the GC peak elution.

3.4. Temperature dependence

The temperature dependence of the electron-capture coefficient, as obtained with a radioactive ECD, is well documented. [36–38]. The temperature dependence can take on unique relationships in a graph of $\ln KT^{3/2}$ versus $1/T$ and these can be used to characterize the nature of the electron-capture process [39]. In order to further evaluate the similarities between the radioactive and non-radioactive ECDs, various compounds have been selected that should display the different electron-capture processes. As mentioned previously, the temperature dependence is the most discerning property in evaluating the similarity between the radioactive and non-radioactive ECDs.

The equation for the electron-capture coefficient, using a constant low voltage in the PDECD, was given in Eq. (23)

$$K = \frac{k_1}{(k_D[D^+] + \mu\nu/A)} \frac{(k_{N_1}[D^+] + k_2)}{(k_{-1} + k_2 + k_{N_1}[D^+])} \quad (33)$$

This equation is identical to that for the radioactive ECD with the exception of the $\mu\nu/A$ term added to $k_D[D^+]$. At low voltages ($<$2–3V), the $\mu\nu/A$ term is small compared to $k_D[D^+]$ and Eq. (33) is essentially equivalent to the electron-capture coefficient for the radioactive ECD.

The effect of the $\mu\nu/A$ term can be evaluated by examining the relationship between the standing current and the voltage across the electron-capture region. These data were given in a previous publication [32] where the voltage above the photoionization region, ν_1, was set at -25 V and the voltage above the electron-capture region, ν_2, was varied from zero to -10 V. The relationship between the standing current and ν_2 can be arrived at by substituting Eq. (10) into Eq. (21) $\nu_b = \nu_2$

$$I_b = \frac{\mu\nu_2}{A} V\, 96\,500 \frac{k_p I[D]}{k_D[D^+] + \mu\nu_2/A} \quad (34)$$

Taking the reciprocal

$$\frac{1}{I_b} = \frac{Ak_d[D^+]}{96\,500\mu V k_p I[D]} \frac{1}{\nu_2} + \frac{1}{96\,500 V k_p I[D]} \quad (35)$$

A graph of $1/I_b$ versus $1/\nu_2$ should be linear. Such a graph is given in Fig. 4. The graph is linear at voltages from 1.5 to 10 V, but is non-linear at lower voltages where the observed current is less than that expected from the linear $1/I_b$ versus $1/\nu_2$ relationship. The intercept $= b = 0.017$ and the slope $= m =$ 0.1087, gives

$$\frac{m}{b} = \frac{k_D[D^+]}{\mu/A} = 6.4 \quad (36)$$

When $\nu_2 = 6.4$ V, the two terms $k_D[D^+]$ and $\mu\nu_2/A$ will be equal.

In this same publication [32], the electron-capture response $(I_b - I_e)/I_{e^-}$ was measured as a function of ν_2 for fixed quantities of $CFCl_3$ and CH_3Br (Fig. 2d in Ref. [32]). The response decreases with voltage as one would expect from Eq. (33). In any event, if $\nu_2 =$ constant, then the electron-capture coefficient will be constant. If ν_2 is small, then the electron-capture coefficient defined by Eq. (33) will be equivalent to that for the radioactive ECD. The temperature dependence of K depends upon k_1, k_{-1}, k_2, and k_{N_1} $[D^+]$ and these will be independent of ν_2.

The temperature dependence of K in the PDECD has been presented previously [31–33]. In previous publications regarding the radioactive ECD, we have included another reaction step, which is a direct dissociative electron-capture process

$$AB + e^- \rightarrow A + B^- \quad (37$$

and a rate constant k_{12} has been associated with this reaction step. This is analogous to electron attachment to AB followed by *rapid* dissociation

$$AB + e^- \xrightarrow{k_1} AB^- \xrightarrow{k_2} A + B^- \quad (38)$$

For simplicity in the analysis of the non-radioactive ECD, we will eliminate k_{12} and assume that this process occurs when k_2 is large, as assumed in reaction step (38).

The expression for the electron-capture coefficient in Eq. (33) contains rate constants that have different temperature dependencies and when the temperature of the ECD is changed from say 30 to 350°C, these

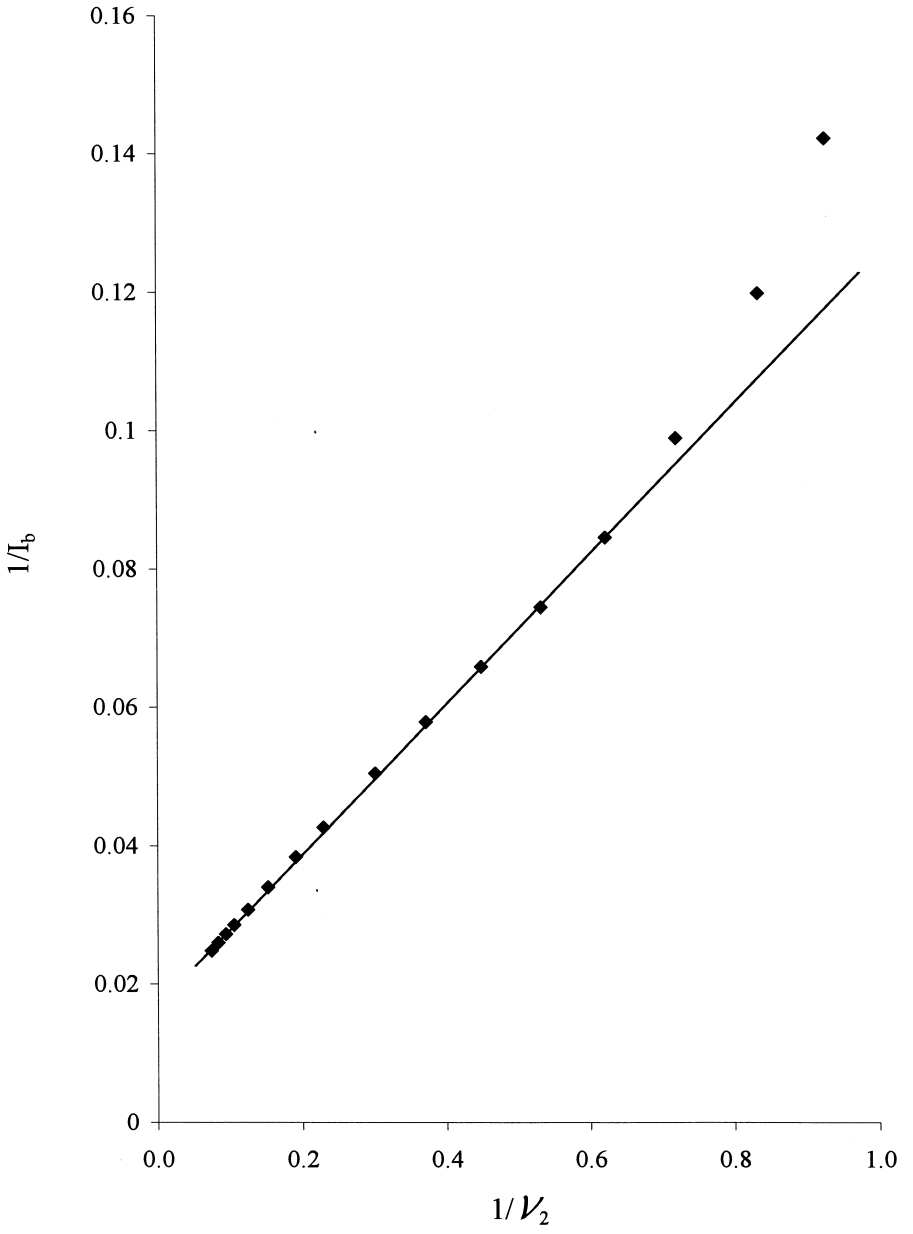

Fig. 4. Graph of $1/I_b$ versus $1/\nu_2$.

rate constants can change dramatically. Consequently, the second ratio on the right side of Eq. (33)

$$\frac{(k_{N_1}[D^+] + k_2)}{(k_{-1} + k_2 + k_{N_1}[D^+])} \tag{39}$$

can change dramatically when the dominant rate constants prevail. In particular k_{-1}, k_2, k_{N_1} $[D^+]$ can change the order of their magnitudes as the temperature is changed and this gives rise to different kinetic mechanisms. These have been well documented [39] but, for convenience to the reader, we will review them at this time. The Greek symbol associated with each mechanism bears no order and we have retained

the same nomenclature that prevails in the literature. The sequence of the mechanisms as given below is of the order of high temperature to low temperature. In the following, we assume the terms $(k_D[D^+]+\mu\nu/A)$ and $k_{N_1}[D^+]$ are independent of temperature. E^* is the Arrhenius activation energy and E_i^* are the activation energies of the individual reaction steps.

δ-region:

$$k_2 > k_{-1} > k_{N_1}[D^+]$$

$$K = \frac{k_1}{k_D[D^+] + \mu\nu/A}, E^* = E_1^*$$

γ-region:

$$k_{-1} > k_2 > k_{N_1}[D^+]$$

$$K = \frac{k_1 k_2}{(k_D[D^+] + \mu\nu/A)k_{-1}}, E^* = E_1^* + E_2^* - E_{-1}^*$$

α-region:

$$k_{-1} > k_{N_1}[D^+] > k_2$$

$$K = \frac{k_{N_1}[D^+]k_1}{(k_D[D^+] + \mu\nu/A)k_{-1}}, E^* = E_1^* - E_{-1}^*$$

β-region:

$$k_{N_1}[D^+] > k_{-1} > k_2$$

$$K = \frac{k_1}{k_D[D^+] + \mu\nu/A}, E^* = E_1^*$$

In the α-region, the temperature dependence is dependent on the ratio k_1/k_{-1}, which is the equilibrium constant for the electron attachment to form a stable negative ion.

$$e^- + AB \underset{k_{-1}}{\overset{k_1}{\rightleftarrows}} AB^- - \Delta E = EA$$

We can apply the statistical thermodynamic equilibrium expression

$$K_{eq} = \frac{f_{AB^-}}{f_{e^-} f_{AB}} e^{EA/RT} = \frac{f_{AB^-}}{(2\pi m_e kT)^{3/2} f_{AB}} e^{EA/RT}$$

where f_i are partition junctions, m_e = mass of the electron, k = Boltzmann constant and EA is the electron affinity. The partition function for the electron contains a $T^{3/2}$. Consequently, if the ratio f_{AB}^-/f_{AB} is assumed to be constant, then $\ln K_{eq} T^{3/2}$ should be linear with $1/T$. For this reason, we graph $\ln KT^{3/2}$ versus $1/T$, where K is the electron-capture coefficient

$$K = \frac{k_{N_1}[D^+]}{(k_D[D^+] + \mu\nu/A)} K_{eq}$$

The slope of this graph in the α-region will be equal to EA/R. The graph of $\ln KT^{3/2}$ is justified for only the α-region, but for simplicity, we continue to use this graph throughout. The slope for the other regions can be related to E^* by

$$\text{slope} = \frac{E^*}{R} + \frac{3}{2}\bar{T}$$

where $\bar{T}$ is some average T over that region. In order to assist in understanding the consequences of the various regions on the temperature dependence, we will illustrate how $\ln KT^{3/2}$ versus $1/T$ would look if *all* regions were experienced by a single compound. This is not generally true in that, frequently, only one or two regions are observed. These will be illustrated later in terms of practical situations. A hypothetical graph of $\ln KT^{3/2}$ versus $1/T$ is given in Fig. 5. The intercepts, corresponding to the linear relationship for each region, are representative of what one might expect, but there are considerable variations from one compound to another. In this hypothetical case, the negative ion, AB^-, is assumed to dissociate. Note that, at low temperatures (high $1/T$), the β-region displays a small, negative slope corresponding to the activation energy for electron attachment to form AB^-. This activation energy can be associated with some geometrical change in order to form the negative ion, which has a different structure from the neutral molecule, AB. For larger molecules, the addition of an electron causes very slight changes in molecular structure since the molecular orbital in which the added electron resides is spread out over the large space of the molecule. Since the molecular orbital is so diffuse, the added electron has little effect on the bond energies. On the other hand, in smaller molecules the added electron can influence bond energies and molecular structure and the activation energy for attachment can be significant. Note that the same temperature dependence should be

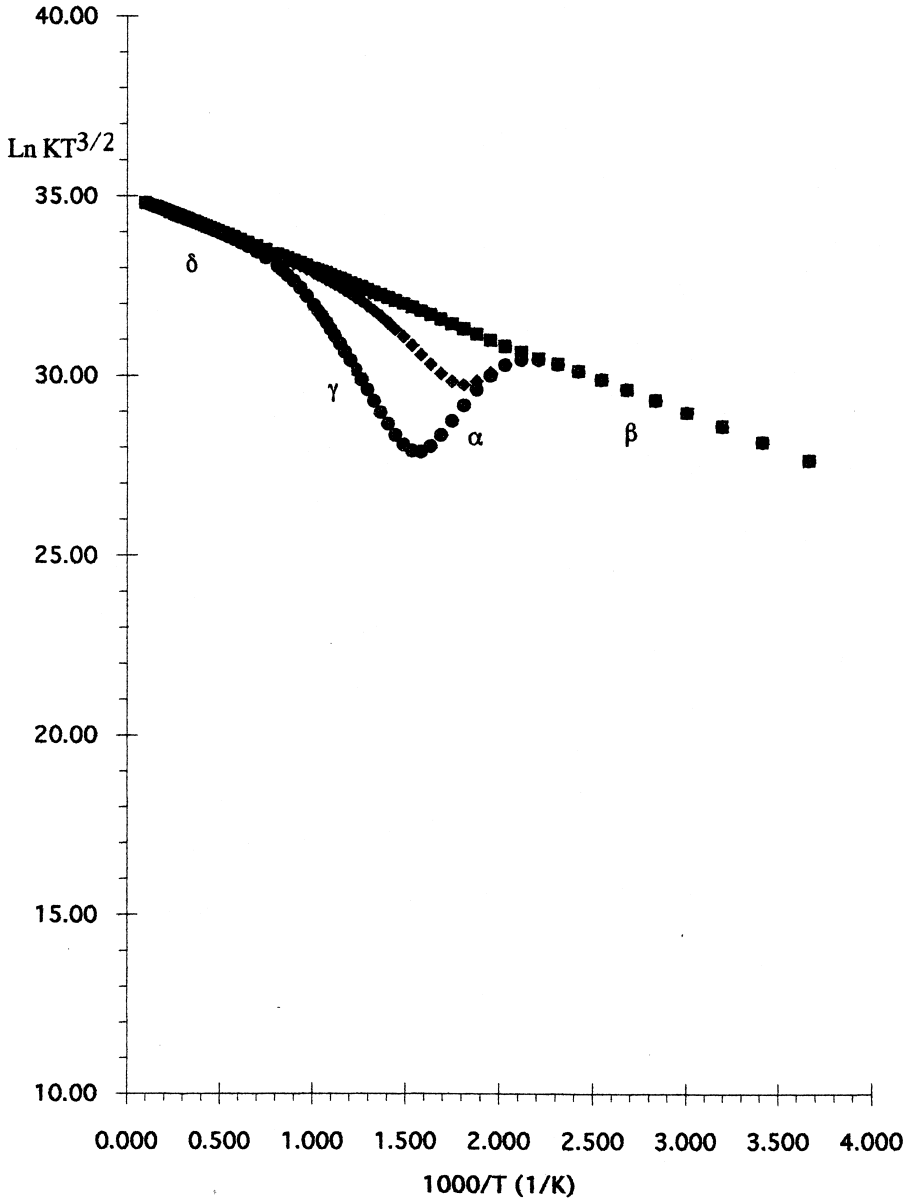

Fig. 5. Graph ln $KT^{3/2}$ versus $1/T$ showing four possible linear regions. $E_2^*=25$ kcal (■), $E_2^*=30$ kcal (♦), $E_2^*=35$ kcal (●).

observed for the δ-region. The difference between the δ-region and the β-region is that AB^- leads to dissociation in the δ-region whereas the AB^- should be stable in the β-region. In the δ-region, dissociation is assumed to be rapid, which simulates the k_{12} reaction step given in Eq. (37).

In the α-region, the dissociation of AB^- is sufficiently difficult at this temperature that only electron detachment is significant. Consequently, the electron attachment–detachment equilibrium is established from which the electron affinity can be calculated from the slope. In many molecules, dis-

sociation of the negative ion is negligible and only the α-region and possibly the β-region at lower temperatures is observed.

In the γ-region, the molecular negative ion has a significant lifetime before dissociation and one can observe the temperature dependence on all three rate constants, k_1, k_{-1} and k_2. In order to observe the γ-region, E_2^* must be greater than E_{-1}^*, which is tantamount to saying that the negative ion is in a reasonably deep potential well with respect to dissociation as well as electron detachment.

In Fig. 5, we show hypothetical curves for three activation energies for dissociation: $E_2^*=25$, 30 and 35 kcal (1 cal=4.184 J). The activation energy for attachment is taken as $E_1^*=4$ kcal and for detachment as $E_{-1}^*=20$ kcal. Note that there is almost no indication of the formation of a stable negative ion when the $E_2^*=25$ kcal, even though E_2^* is 5 kcal greater than E_{-1}^*. For any $E_2^*<25$ kcal, essentially the same ln $KT^{3/2}$ versus $1/T$ linear function is observed. In our previous discussion, we stated that a single dissociative step, Eq. (37), would be analogous to electron attachment to give AB^- followed by a *rapid* dissociation into $A+B^-$, Eq. (38). The curve for $E_2^*=25$ kcal in Fig. 5 is an illustration of this, where a single linear relationship is observed. However, for higher $E_2^*=30$ and 35 kcal, the formation of an intermediate stable negative ion is very evident by the positive slope in the α-region, where the slope is related to the EA by

$$\text{slope}=\frac{EA}{R}=\frac{-(E_1^*-E_{-1}^*)}{R}$$

The γ-region is then observed at higher temperature and the slope is negative since the E_2^* is greater than the $EA=-(E_1^*-E_{-1}^*)=16$ kcal. If the E_2^* is very large compared to E_{-1}^*, the δ-region may never be observed at the temperatures attainable with the ECD.

Dissociative electron capture is most frequently observed with Cl-, Br- and I-containing compounds since these atoms have relatively low C–X bond energies but high atomic electron affinities. The C–X bond energies are strongly affected by the adjacent groups bonded to the carbon. The chloromethanes are a good example of the effect of adjacent halogens on the carbon in the C–X bond. The chloromethanes CCl_4, $CHCl_3$ and CH_2Cl_2 were run in two prior studies with the non-radioactive ECD [31–33] using CH_4 as the dopant. These were also run using Xe as dopant in a more recent study [34]. In these molecules, one expects immediate dissociation since the aliphatic halide would not be expected to form a stable negative ion. Linear graphs of ln $KT^{3/2}$ versus $1/T$ were observed in all cases. The slopes and intercepts for each linear relationship are given in Table 2. Note the good consistency between the various PDECD studies and also with the radioactive ECD.

The polycyclic aromatic hydrocarbons generally have low energy molecular orbitals that can accept an electron to form a stable negative ion. The reason for this stability is the delocalized nature of the molecular orbital. When a halogen is attached to an aromatic hydrocarbon, potentially, one may form a molecular negative ion that subsequently could dissociate to give the halogen negative ion. Benzene does not have molecular orbitals that are sufficiently delocalized and with low enough energy to form a negative ion. However, with chloro substituents, the molecular orbitals are lowered in energy and capable of forming a negative ion.

In Figs. 6 and 7, we show the temperature

Table 2
Comparison of temperature dependence of chloromethanes

Detector	Dopant	CCl_4		$CHCl_3$		CH_2Cl_2	
		Slope	Intercept	Slope	Intercept	Slope	Intercept
PDECD [23]	CH_4	−0.07	34.4	−1.40	35.0	−3.51	32.5
PDECD [32]	CH_4	−0.02	34.5	−1.43	34.6	−3.62	30.9
PDECD [34]	Xe	−0.065	33.6	−1.87	34.2	−4.44	33.2
ECD (radioactive) [40]	CH_4	−0.096	33.8	−2.13	35.5	−4.37	33.9

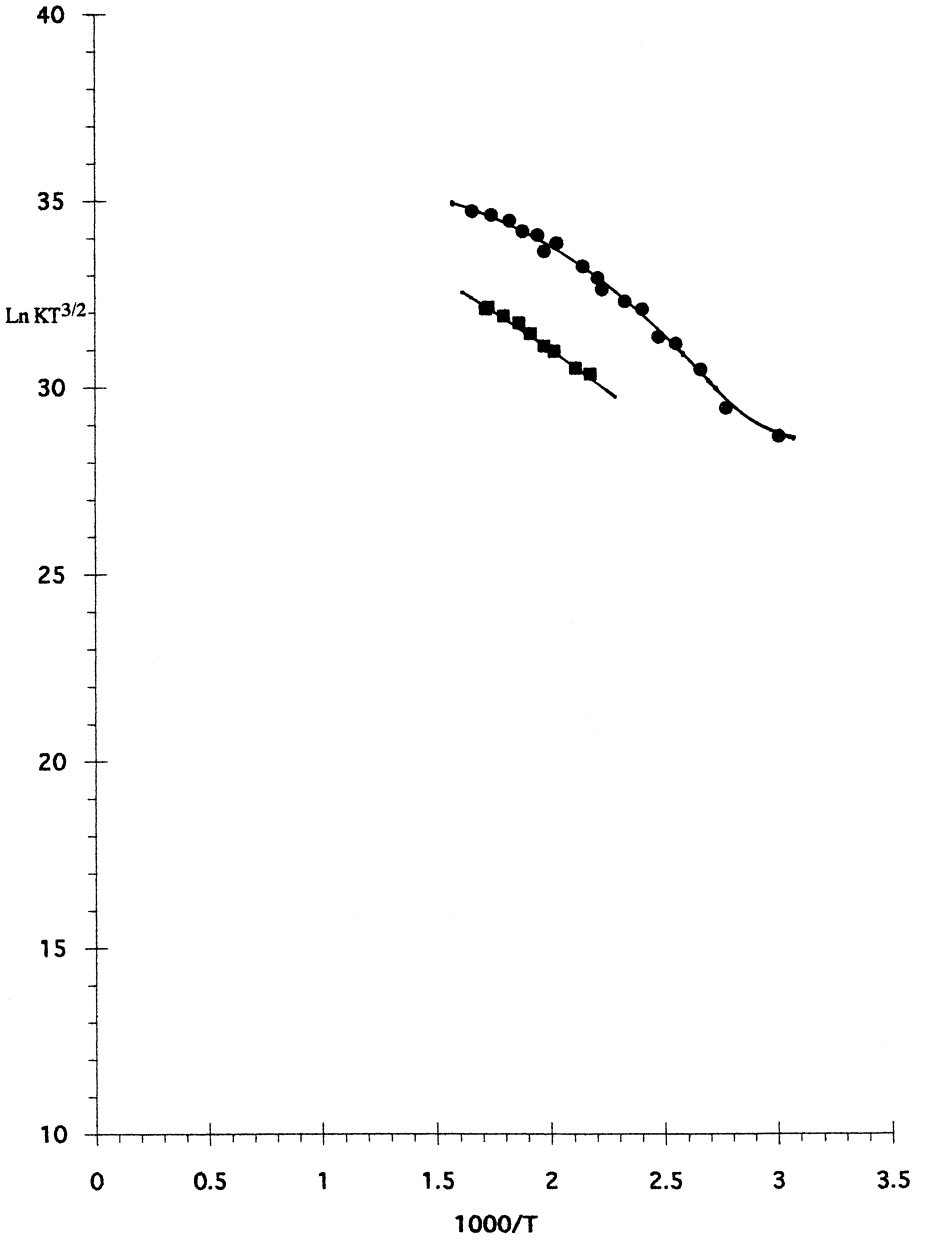

Fig. 6. Graph of ln $KT^{3/2}$ versus $1/T$ for 1,2-dichlorobenzene (■) and 1,3,5-trichlorobenzene (●).

dependence for four chlorobenzenes as obtained with the PDECD [33]. In Fig. 6, we show 1,2-dichlorobenzene and 1,3,5-trichlorobenzene, both of which show a δ-region followed by the start of a γ-region where the negative slope is of a larger magnitude. One would expect the electron affinity of the molecule to increase with increasing chloro substitution and this is consistent with the data in Figs. 6 and 7. The data for 1,2-dichlorobenzene is continuing to break downward with decreasing T (increasing $1/T$) whereas 1,3,5-trichlorobenzene appears to be just beginning the α-region as there is a slight increase at

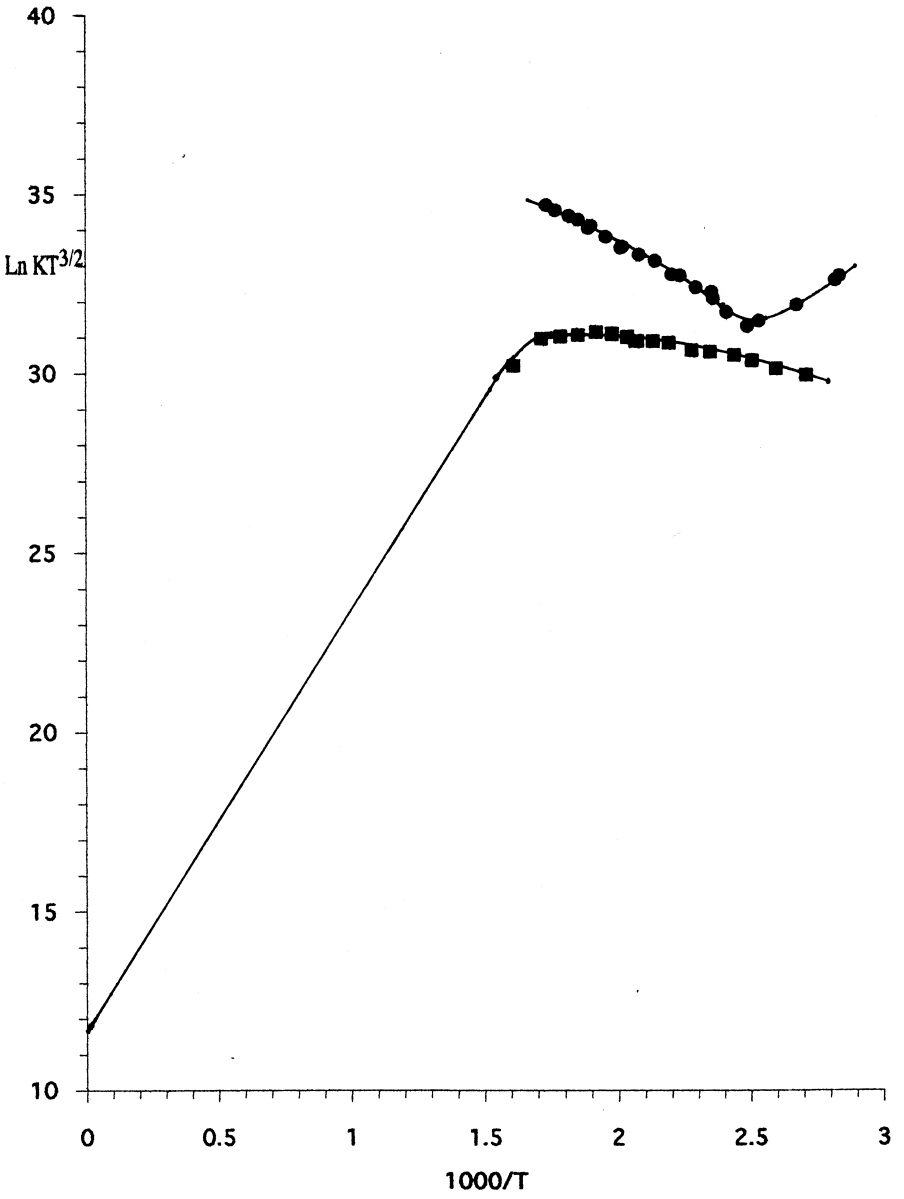

Fig. 7. Graph of ln $KT^{3/2}$ versus $1/T$ for 1,2,4,5-tetrachlorobenzene (●) and hexachlorobenzene (■).

the lowest temperature. 1,2,4,5-Tetrachlorobenzene goes through the δ- and γ-regions and breaks up into the α-region at low temperatures. This is consistent with the expected higher *EA* compared to the di- and trisubstituted chlorobenzenes.

Hexachlorobenzene would also be expected to dissociate into Cl^-. However, due to the stability of the $C_6Cl_6^-$, as evidenced by its high electron affinity of ~1 eV, the activation energy for this dissociation would be high. Consequently, the dissociation would occur only at much higher temperatures, higher than those used to obtain the data in Fig. 7 and the electron-capture shows only the α- and β-regions.

As mentioned earlier, benzene does not have sufficiently low energy π orbitals to form a stable negative ion and does not capture electrons. How-

ever, when a C=O group is conjugated to the phenyl ring, the lowest unoccupied orbital is sufficiently lowered to form a stable negative ion and give a moderate EC response. The temperature dependence of the electron-capture coefficient for acetophenone and benzaldehyde using the PDECD with CH_4 as dopant is shown in Fig. 8. Since the electron affinity for these molecules is low, only an α-region is observed. The temperature dependence for these compounds closely parallels that obtained with a radioactive ECD. The slopes for the graphs in Fig. 8 give the electron affinities and these are compared to those obtained with the radioactive ECD in Table 3.

As mentioned earlier, the use of H_2 as dopant in

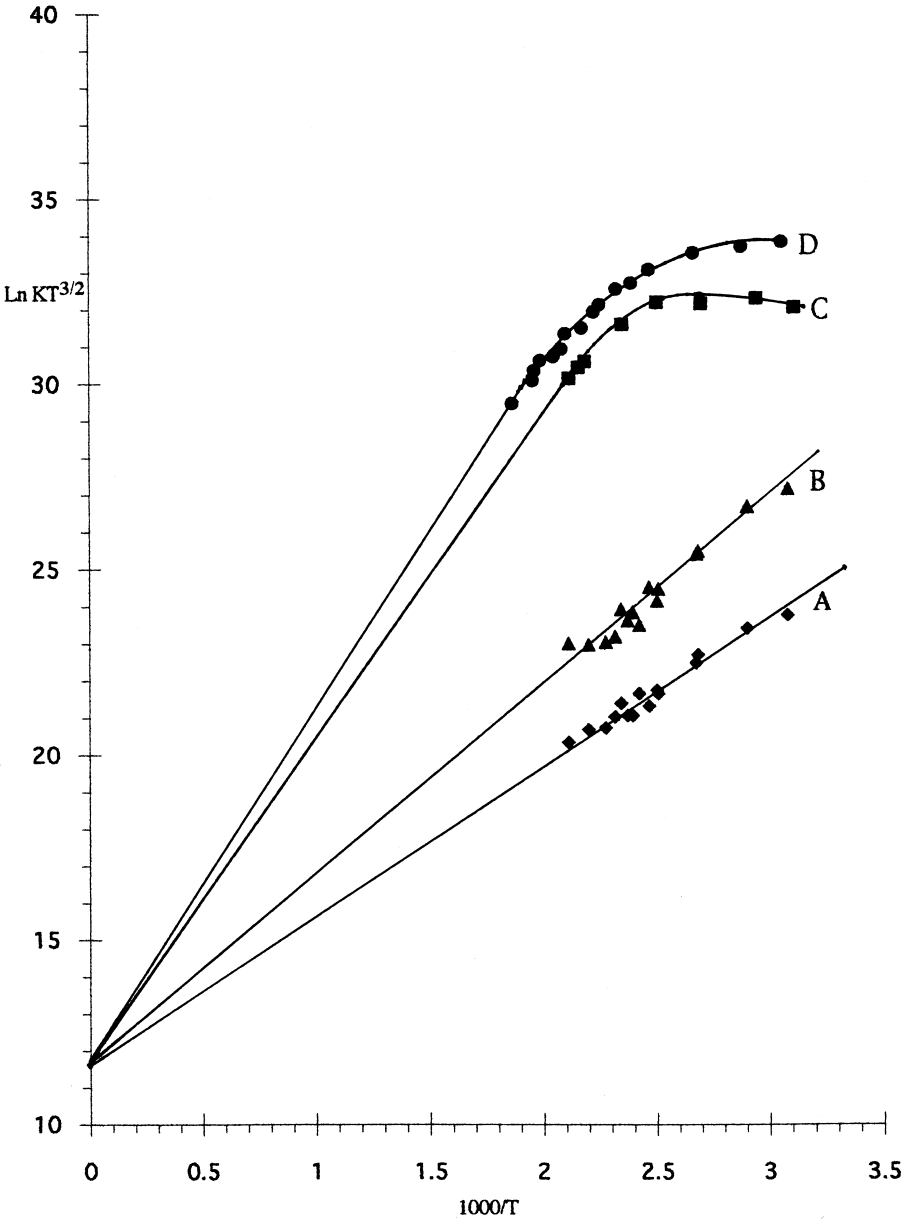

Fig. 8. Graph of ln $KT^{3/2}$ versus $1/T$ for acetophenone (A), benzaldehyde (B), biacetyl (C) and hexafluorobenzene (D).

Table 3
Comparison of electron affinities obtained with the PDECD and the radioactive ECD

Compound	Electron affinity (*EA*)		Other techniques		
	PDECD	Radioactive ECD [29]	EA	Method	Ref.
Acetophenone	0.33±0.01	0.334±0.006	0.35±0.1	Half wave reduction pot.	[44]
Benzaldehyde	0.44±0.02	0.430±0.008	0.45±0.1	Half wave reduction pot.	[44]
Biacetyl	0.74	0.63±0.05	0.69±0.1	Thermal charge transfer	[42,43]
C_6F_6	0.89	0.83±0.022	0.8±0.1	Photoelectron spectroscopy	[45]

the PDECD gives much lower electron-capture coefficients for these molecules, which differ greatly from the radioactive ECD results. The use of CH_4 as dopant is apparently critical in order to obtain electron attachment to molecules with only moderate electron affinities. It is possible that the electron attachment cross sections for these molecules are especially large at low electron energies and only CH_4 is capable of obtaining such low energies with a thermal distribution of electron energies.

Biacetyl gives a relatively strong ECD response as a result of forming a stable negative ion. The temperature dependence of the electron-capture coefficient obtained with the PDECD is also shown in Fig. 8. The data clearly show an α-region followed by a β-region at lower temperatures. The β-region will only be observed when the electron affinity is sufficiently high so that k_{-1} is sufficiently low to make $k[D^+] >> k_{-1}$. In this case, there are no fragment radicals with sufficient electron affinity to promote dissociation, so even at higher temperatures, we would expect a decrease in the electron-capture coefficient with increasing temperature, as shown in the α-region.

Hexafluorobenzene also forms a stable negative ion with an electron affinity in excess of that of biacetyl. Since the C–F bond energy is so stable, there is *no* dissociation into F^- and C_6F_5 at temperatures that are attainable with the radioactive ECD. Consequently, C_6F_6 also shows very clearly the α- and β-regions, as shown in Fig. 8. At lower temperatures in the β-region, the curve should have a zero or negative slope, as shown with biacetyl. However, for C_6F_6 the data define a positive slope in the β-region of lower magnitude than the slope in the α-region. About the only way that this could happen is the existence of another negative ion state of lower energy that potentially would show another α- and β-region. This has been observed previously in the case of CS_2 [41]. The electron affinity for the $C_6F_6^-$ state observed in Fig. 8 is 0.89 eV. A lower electron affinity of 0.52 eV has been reported for $C_6F_6^-$ from thermal electron transfer equilibria [42,43]. Note that, for all four molecules that show an α-region, the PDECD results shown in Fig. 8 closely parallel those of the radioactive ECD.

In order to compare the PDECD results in Fig. 9 with the radioactive ECD, we have evaluated the *EA* from the slopes in the α-region. Comparisons with the previously determined *EA* values using the radioactive ECD are shown in Table 3. In general, there is good agreement between the PDECD and the radioactive ECD. The EA are further supported by estimates from other techniques, as also shown in Table 3.

We conclude this section with the temperature dependence of some pesticides. Pesticide analysis is one of the most important applications of the ECD. For this reason, it is essential that a non-radioactive ECD be as successful as the radioactive ECD in this pursuit. In general, each of the pesticides contains a high percentage of chlorine and, consequently, has a very high electron-capture coefficient. Furthermore, the electron-capture coefficients for all of the pesticides are essentially temperature-independent, indicative of a β-region according to our previously described classification. The temperature dependence is shown in Fig. 9. Since they have electron-capture coefficients of similar magnitude, they are represented on different graphs. In many of the pesticides, the chlorines are weakly bonded and probably undergo dissociative electron capture to $C1^-$, but this cannot be concluded on the basis of the temperature dependence. It is interesting to note that the measurements could be extended down to temperatures of the order of 160°C, despite the high boiling points for

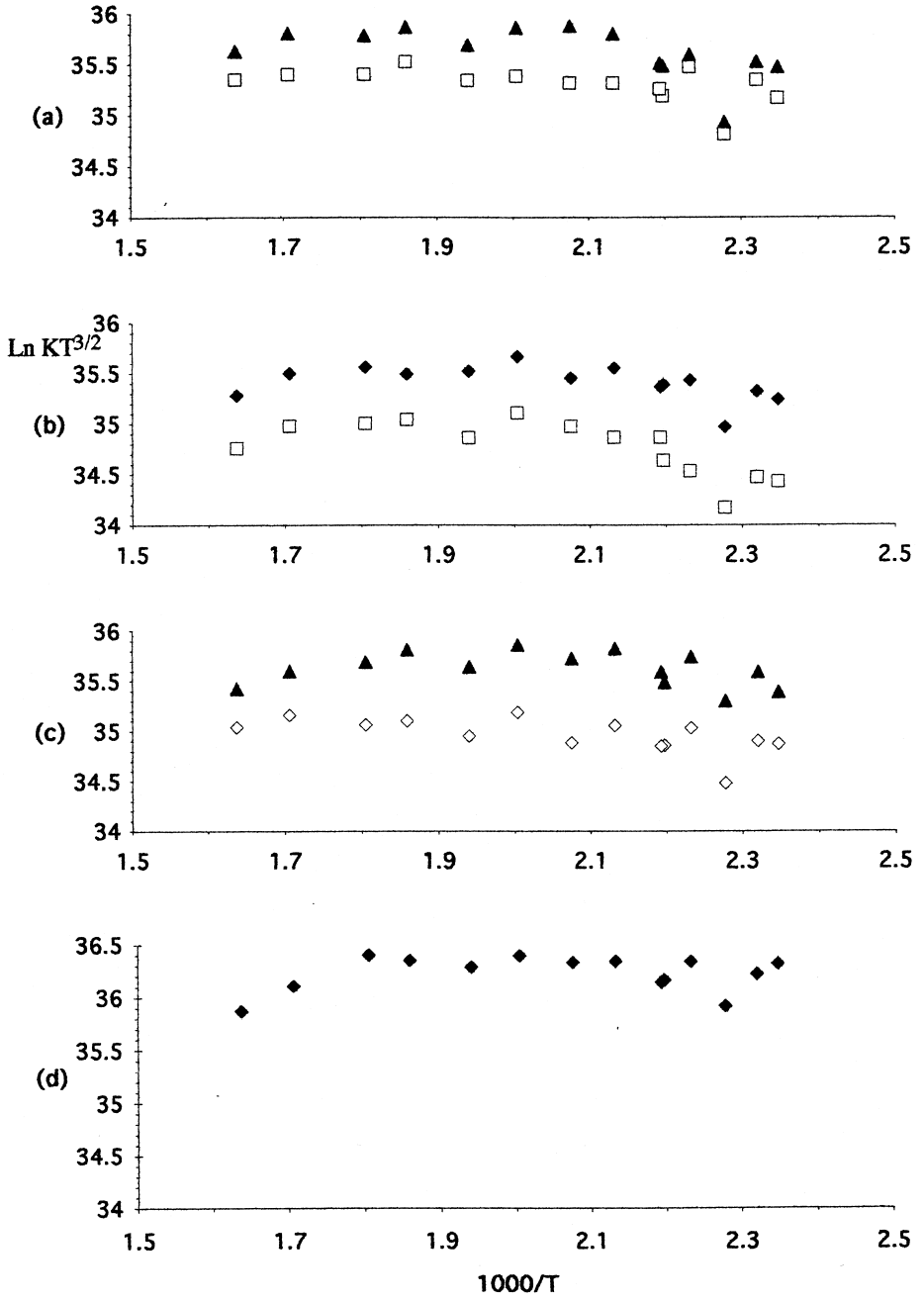

Fig. 9. Graph of ln $KT^{3/2}$ versus $1/T$ for some pesticides: (a) Heptachlor (▲), *p,p′*-DDT (□); (b) heptachlor-epoxide (♦), dieldrin (□); (c) aldrin (▲), endrin (◇) and (d) lindane (♦).

the pesticides. This gives an indication of the 'inertness' of the detector in that the surface of the sapphire insulators is non-adsorbing.

A linear regression analysis has been performed on the data in Fig. 9. The slopes and intercepts, for the pesticides shown in Fig. 9, are given in Table 4,

Table 4
Slopes and intercepts for the temperature dependence of some pesticides

Pesticide	Slope$\pm\sigma_{slope}$	Intercept$\pm\sigma_{intercept}$
Heptachlor	0.20±0.15	34.77±0.30
p,p′-DDT	−0.23±0.23	35.11±0.47
Heptachlor-epoxide	0.68±0.19	34.70±0.38
Dieldrin	0.26±0.17	34.76±0.34
Endrin	0.10±0.14	34.62±0.29
Aldrin	0.42±0.19	34.62±0.40
Lindane	0.55±0.19	34.25±0.39

along with the associated errors. The slopes are essentially zero when one considers that the $T^{3/2}$ term causes a positive slope of $3/2\ \bar{T}$~600 K. The constancy of the intercept at ~34.7 indicates the constancy of the electron-capture coefficients.

4. Use of a pulsed discharge photoionization detector in conjunction with a pulsed discharge electron-capture detector

The non-radioactive PDECD can be converted to a PDPID by simply removing the methane dopant and changing the potentials on the bias electrodes. In order to do this rapidly, we do not change the electrometer/bias electrode positions. The methane dopant is removed by a four-way valve in which a low flow of helium from the detector purges the transfer line. The configuration is:

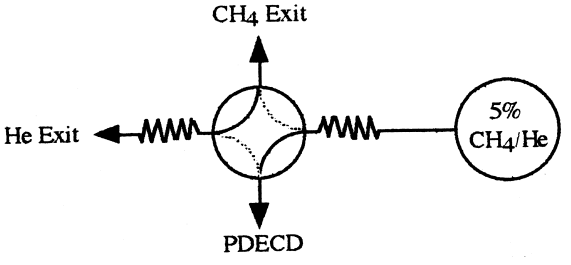

The restrictor for the He exit is not very restrictive so that the flow through the exit port is ~1 ml/min. This flow-rate will depend upon the pressure of the detector, which is slightly over 1 atm. The pressure of the detector will depend on the exit tube from the detector, which is necessary to prevent back diffusion of air. Note that in the He-PDPID operation, a low flow of helium is passing through the transfer line from the detector to this four-way valve. The transfer line is cleared of CH_4 much more rapidly in this configuration rather than adding He to the four-way valve to clear the transfer line. The change from the He-PDPID to the PDECD mode is rapid since the added methane (5%) is at a flow-rate of ~3.5 ml/min and the transfer line will equilibrate to the methane quickly within the tolerances for the CH_4 concentration.

In a previous publication [46], two important uses of the He-PDPID in conjunction with the PDECD were described: (1) Rapid switching between these detectors in order to selectively use either detector during a chromatogram and (2) use of the He-PDPID to identify the major component in an initial PDECD investigation of a compound. Switching from one mode to the other was accomplished in 4–6 s and this is demonstrated in Fig. 10. The upper chromatogram uses the He-PDPID, which is equivalent to the previously designated PDHID, and peaks 2–6 have a low response or they are obscured by the large solvent peak. Peak 9 is not distinguishable from the solvent tail and an impurity peak ‘a’ is barely noticeable. The middle chromatogram uses the PDECD and it shows a weak response for peaks 1, 7 and 10, but a much stronger response for the other compounds and essentially no response for the solvent. The lower chromatogram shows the combined use of both detectors and five switches from one mode to the other in order to utilize the most sensitive response from each detector.

In Fig. 11 we show the PDECD response to a sample containing principally *cis*- and *trans*-1,2-dichloroethylene. However, since both *cis* and *trans*-1,2-dichloroethylene are weak electron-capturers, their PDECD peaks are not the major peaks. This happens quite commonly where strongly capturing impurities give a much greater response and it is virtually impossible to identify the weakly capturing major components. However, a second chromatogram, which is run under identical conditions using the He-PDPID mode, clearly identifies the major components and obviously gives no significant response to the impurities at the sensitivity required to give a significant response for the major components. These chromatograms clearly demonstrate the advantage of using the *same* detector to operate in both modes.

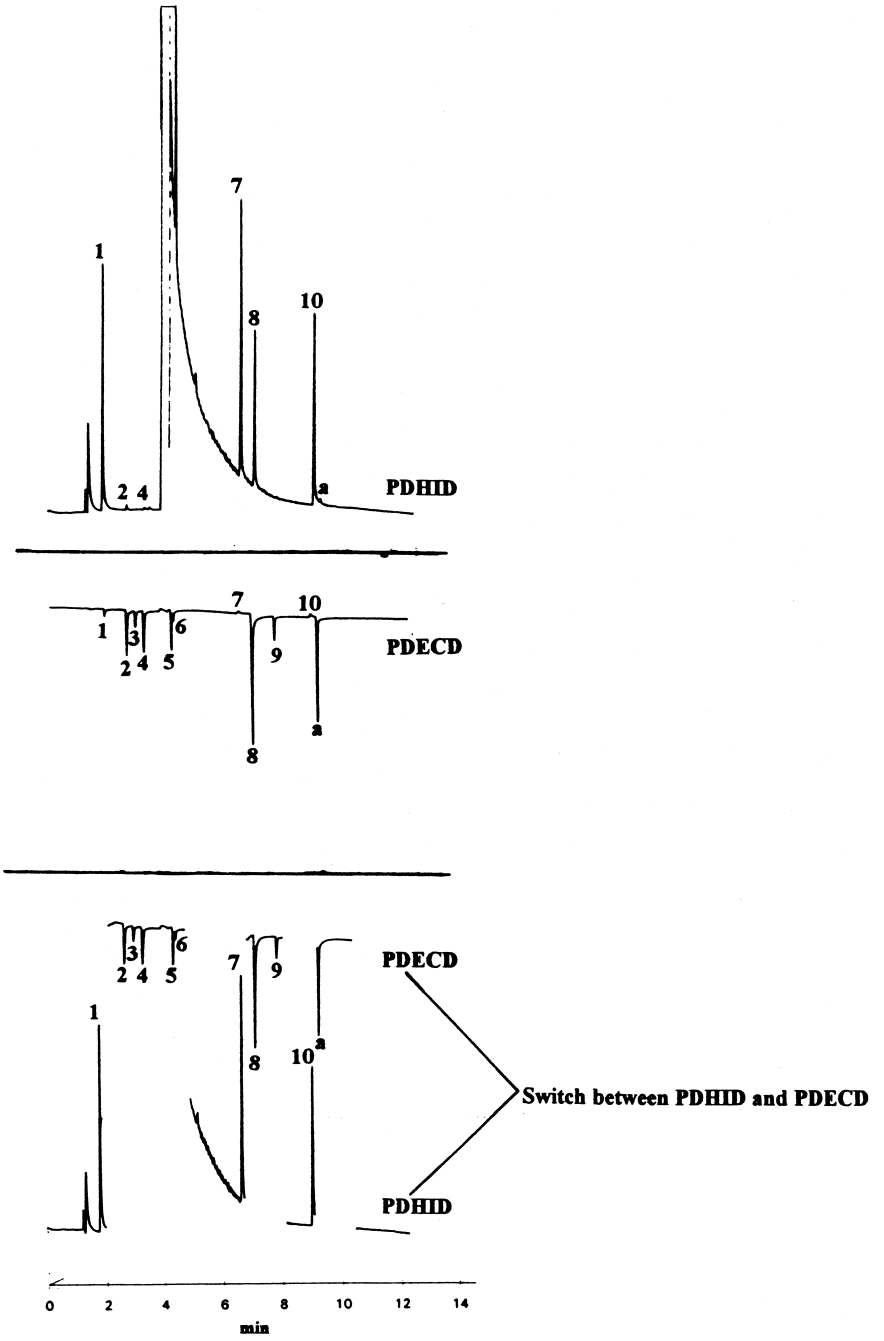

Fig. 10. Chromatogram of alkane–alkene chloro mixture using PDECD/PDHID. Peak number, formula (amount injected): (1) CH_2Cl_2 (3.80 ng); (2) $CHCl_3$ (36.8 pg); (3) 1,1,1-Cl_3CCH_3 (1.67 pg); (4) CCl_4 (0.39 pg); (5) $Cl_2C=CHCl$ (37.0 pg); (6) $ClCH_2ClCHCH_3$ (2.90 ng); (7) toluene (2.20 ng); (8) Cl_2CHCH_2Cl (1.80 ng); (9) $Cl_2C=CCl_2$ (0.38 pg); (10) ClC_6H_5 (2.90 ng) and (a) unknown from compound 8.

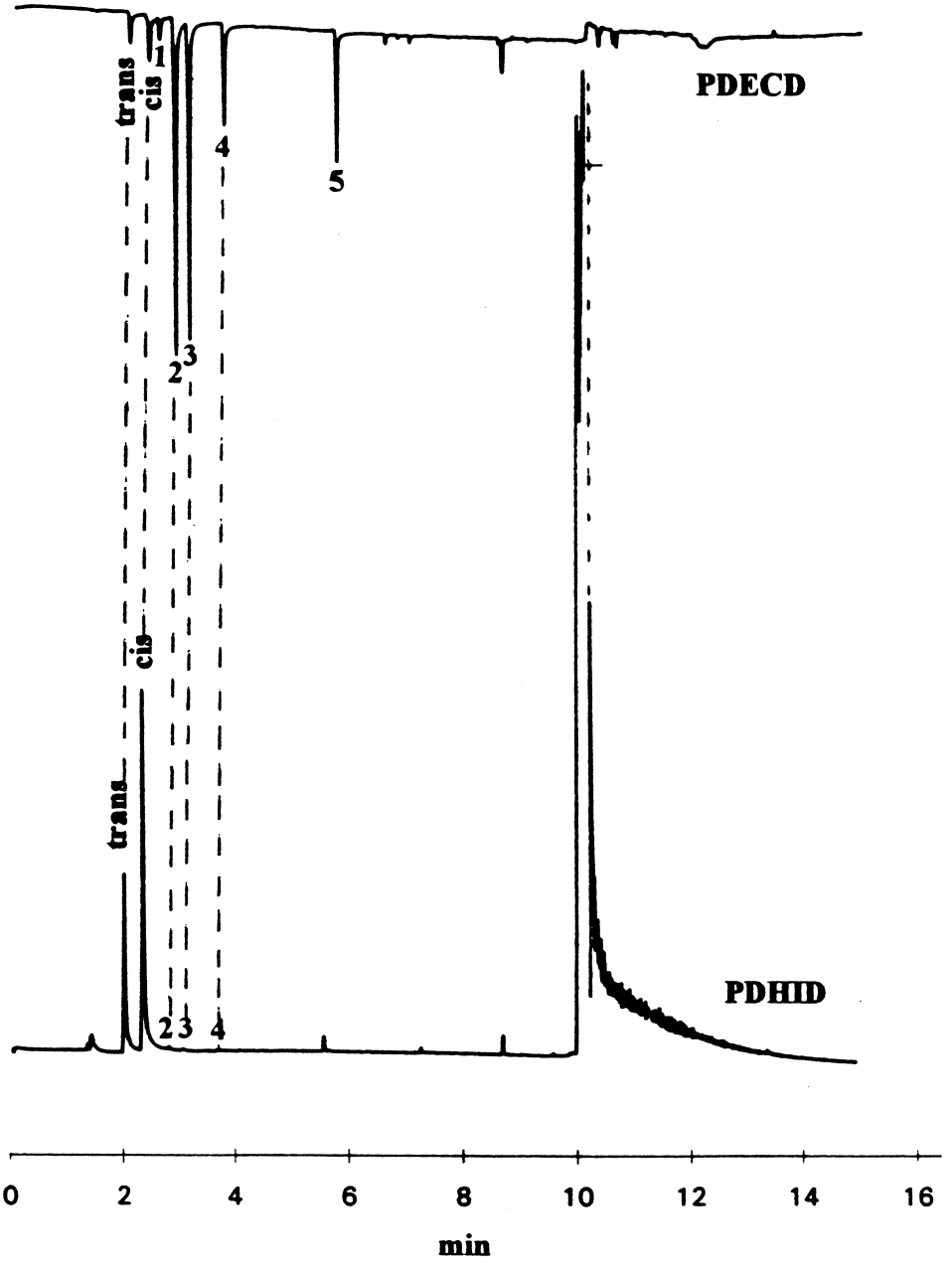

Fig. 11. PDECD/He–PDPID chromatograms of *cis*- and *trans*-1,2-dichloroethylene in undecane. Impurities: (1) $CHCl_3$, (2) 1,1,1-Cl_3CCH_3, (3) CCl_4, (4) $Cl_2C=CHCl$ and (5) $Cl_2C=CCl_2$.

5. Applications

5.1. Pesticides

Pesticide analysis using the PDECD has been investigated throughout the development of the detector. The earlier studies [20] used PEEK and Vespel as insulators and this seriously limited the analysis of pesticides due to the upper temperature limit of 175°C and the somewhat reactive surfaces of

the materials. The subsequent use of sapphire insulators in the electron reaction zone is most important for pesticide analysis since the sapphire allows temperatures of 400°C to be used for ECD operation [32]. Pesticide analysis presents somewhat of a dilemma in that their high boiling points require higher temperatures but their fragile structures are better preserved at low temperatures. For this reason, the inertness of the detector is important so that lower temperatures can be used and, at the same time, the integrity of the chromatography can be maintained. The PDECD has been used in the development of a fast screening method for organochlorine pesticides in water by solid-phase microextraction with fast chromatography [47].

Pesticide analysis using the PDECD has been compared with the use of ^{63}Ni-ECD [32]. One of the comparative chromatograms is shown in Fig. 12. The chromatograms are very similar except for TCMX and endosulfan sulfate, where the response with the non-radioactive PDECD is about 0.6 that from the ^{63}Ni-ECD. In general, the PDECD sensitivity is comparable with that for the ^{63}Ni-ECD. In this study [32], the minimum detectable quantity (MDQ) ($S/N=2$) for the pesticides using the PDECD ranges from 35–100 fg. The value for the often quoted lindane is 36 fg. These MDQ values are high considering the large value for the electron-capture coefficients shown in Fig. 9. This is due to the inordinately high noise level associated with pesticide analysis. This noise is a result primarily of impurities or decomposition products of the pesticides eluted during the course of the chromatogram and is common to both the PDECD as well as the ^{63}Ni-ECD. In a more recent study [35], the MDQ for lindane using the PDECD has been reduced to 16 fg. In general, the MDQs for the pesticides are an order of magnitude higher than the MDQs for lower boiling compounds with comparable electron-capture coefficients.

The linear range of the PDEDC response extends to ~30–80 pg for the pesticides, giving a linear dynamic range of three orders of magnitude [32]. This linear range for the pesticides is about one order of magnitude less than that for lower boiling compounds that are easier to chromatograph. This is primarily due to the higher MDQ values for the pesticides. In a more recent study [35], the linear dynamic range for the pesticides has been extended to 10^4 and that for the lower boiling compounds to 10^5. This is due to the more accurate measurement of change in voltage required in the constant-current mode.

5.2. Polychlorinated biphenyls

Another important analysis commonly performed by the ECD is the GC analysis of polychlorinated biphenyls (PCBs). Whereas each of the pesticides contains a large number of Cl atoms and have similar high electron-capture coefficients, the PCBs have a large range of Cl-atoms per molecule and their electron-capture coefficients correspondingly vary over a large range. In Table 5 are the relative electron-capture coefficients for some PCBs, where the number of Cl-atoms/molecule varies from one to eight. The numbering system for the PCBs is

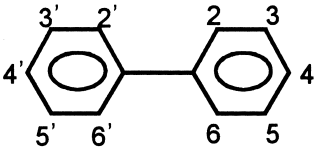

The relative electron-capture coefficients vary by as much as a factor of 100 from 2-chlorobiphenyl to the 2,2′,3,3′,4,4′,6-heptachlorobiphenyl. Note the exceptionally low value for 2-chlorobiphenyl compared to the other PCBs, which show only a small increase with increasing number of Cl-atoms from two to eight per molecule. This is not the same trend as observed with the chlorinated benzenes [31,32].

The structure of biphenyl has the phenyl rings almost coplanar so that the conjugated π system can extend over the entire molecule. Consequently, the lowest unoccupied molecular orbital in biphenyl is considerably lower than in benzene. As a result Cl-substituted biphenyls have a greater tendency to form stable negative ions than the Cl-substituted benzenes. This is evident when one compares the electron-capture coefficients for various PCBs where the Cl-substituents may interfere sterically with one another and possibly distort the coplanarity between the phenyl rings. Note that Cl-substituents in the 2,2′ and/or 6,6′ positions may sterically interfere with one another and the molecule must compensate for this by a slight twist of the phenyl rings. However, the most dominant effect on the electron capture of the PCBs is the *number* of Cl atoms substituted on

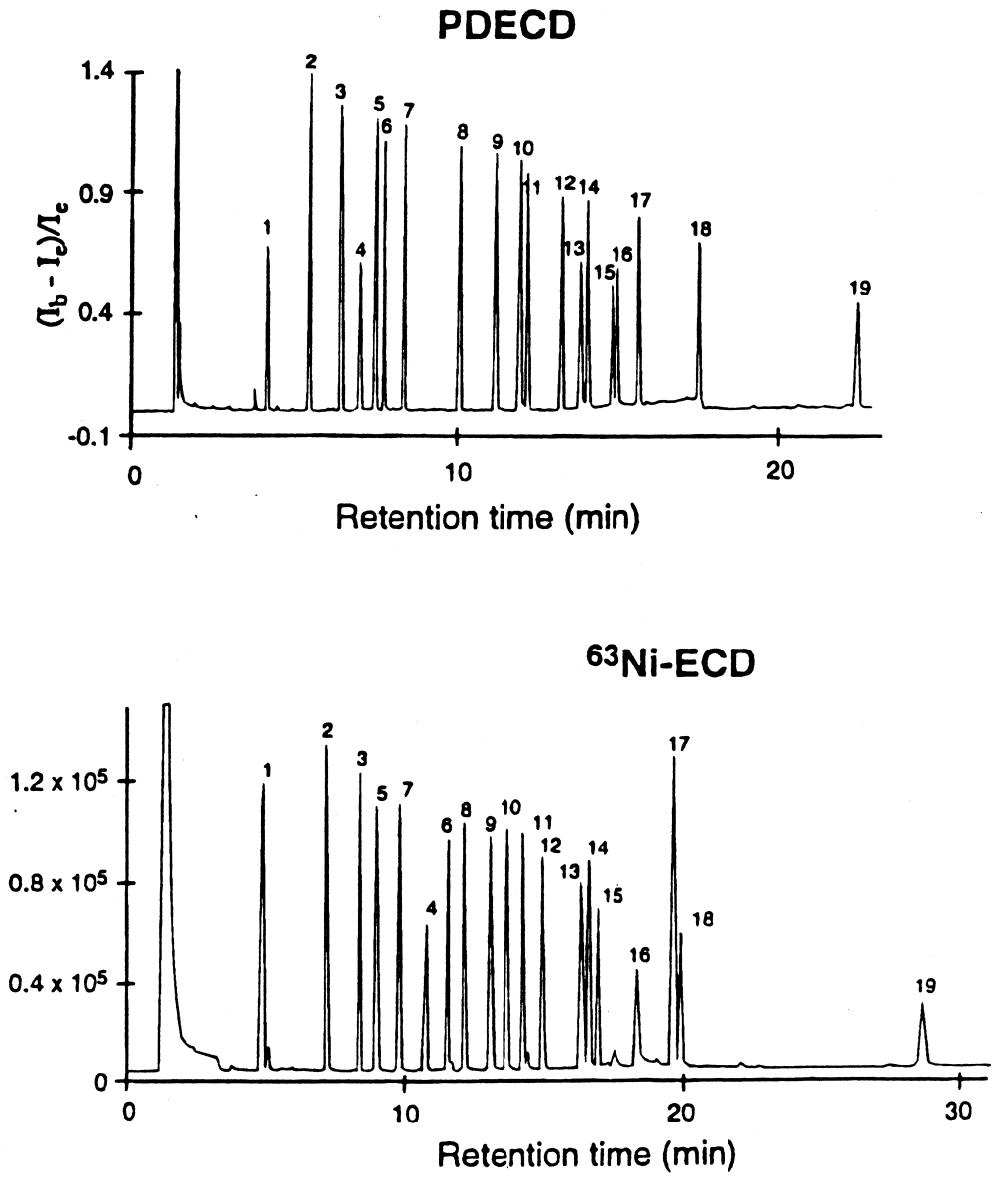

Fig. 12. Comparison of pesticide analysis using the PDECD and ^{63}Ni–ECD. (1) TCMX (surrogate), (2) α-BHC, (3) γ-BHC, (4) β-BHC, (5) heptachlor, (6) δ-BHC, (7) aldrin, (8) heptachlor epoxide, (9) endosulfan I, (10) 4,4′-DDE, (11) dieldrin, (12) endrin, (13) 4,4′-DDD, (14) endosulfan II, (15) 4,4′-DDT, (16) endrin aldehyde, (17) endosulfan sulfate, (18) methoxychlor and (19) DCB (surrogate).

the rings. Examination of the relative electron-capture coefficients in Table 5 shows a general increase with increasing number of Cl substituents. The electron-capture coefficient for the octachlorobiphenyl is apparently diminished due to the 2,2′ and 6,6′ steric hindrance, since its value is close to that of the heptachlorobiphenyl.

The electron-capture coefficients for the PCBs are temperature-dependent, which is quite different from the pesticides where one observes very little tem-

Table 5
Relative electron-capture coefficients for some polychlorinated biphenyls (PCB)

PCB	Relative K^a
2-Chlorobiphenyl	0.8
2,3-Dichlorobiphenyl	12.4
2,4,5-Trichlorobiphenyl	19.4
2,2′,4,4′-Tetrachlorobiphenyl	26.4
2,2′,3,4,5-Pentachlorobiphenyl	35.3
2,2′4,4′,5,6′-Hexachlorobiphenyl	46.8
2,2′,3,3′,4,4′,6-Heptachlorobiphenyl	99.2
2,2′,3,3′,4,5′,6,6′-Octachlorobiphenyl	100.0

[a] Electron-capture coefficients are made relative to 100, which was assigned to 2,2′,3,3′,4,5′,6,6′-octachlorobiphenyl.

perature dependence. This is somewhat understandable since the electron-capture coefficients for the PCBs are less than those for the pesticides, which generally are close to maximum capture, even exceeding CCl_4. Another mixture of the PCBs, containing three to seven chloro substituents, was chromatographed at different detector temperatures. The chromatograms at detector temperatures of 225 and 350°C are shown in Fig. 13. Note that the electron-capture of peaks 1–3 increase with increasing temperature whereas peaks 4–7 decrease with increasing temperature. Also note that an impurity peak just before peak 4 is obvious at 225°C but disappears at 350°C. The temperature dependence for this impurity is similar to that for peaks 4–7, which decrease with increasing temperature. The opposite behavior is observed for the impurity after peak 3, which becomes more apparent at 350°C.

A more quantitative evaluation of the temperature dependence of the PCBs using the non-radioactive ECD is shown in Fig. 14 in the form of the $\ln KT^{3/2}$ versus $1/T$ graphs. Since the data overlap extensively, the behavior of the seven PCBs are shown in three separate graphs. The change in $\ln KT^{3/2}$ is the same for all three graphs but the range is different in order to accommodate the different magnitudes. Peaks 1 and 2 (tri- and tetrachlorobiphenyl) are shown in Fig. 14a and the $\ln KT^{3/2}$ increases with increasing temperature (decreasing $1/T$). The two pentachloro PCBs are shown in Fig. 14b and they show different behavior. The electron-capture of 2,2′,4,5,5′-pentachlorobiphenyl increases with increasing temperature (decreasing $1/T$), similar to the tri- and tetraclorobiphenyls in Fig. 14a. The 2,3,4,4′,5,5′-pentachlorobiphenyl initially decreases with increasing temperature and then increases slowly. Apparently, the 2,2′ steric hindrance causes the 2,2′,4,5,5′-pentachlorobiphenyl to have a significant activation energy for electron attachment in going to the more planar configuration of the negative ion. This steric hindrance is not present in the 2,3′,4,4′,5-pentachlorobiphenyl and it tends to form a negative ion more readily. Peaks 5–7 are shown in Fig. 14c where all three give similar temperature dependence to that for 2,3′,4,4′,5-pentachlorobiphenyl. Based upon our previous discussion of the temperature dependence, we would conclude that peaks 1–3 display regions γ and δ whereas peaks 4–7 display regions α and γ.

From an analytical perspective, one may wish to carry out the PCB analysis with the ECD at two temperatures in order to obtain the maximum sensitivity for all PCBs. At a high temperature (350–400°C), the PCBs with fewer Cl/molecule will have higher electron capture due to enhanced dissociative electron attachment. At low temperature (200–225°C), the more highly Cl-substituted PCBs will have enhanced negative ion formation, which is more favorable at low temperatures. The non-radioactive ECD should be capable of performing the PCB analysis at low temperature since its walls are inert and have little tendency to absorb compounds. This could be important if one desires the maximum sensitivity for the more highly Cl-substituted PCBs.

5.3. Inorganic analysis

Since the very beginning of gas chromatography,

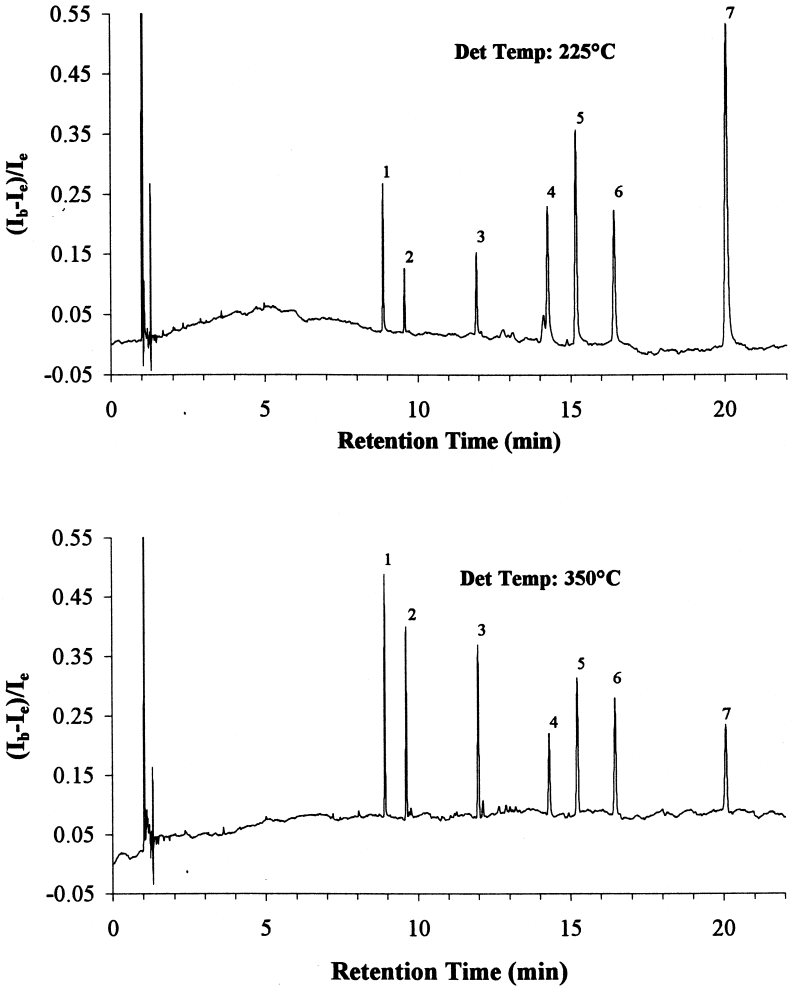

Fig. 13. PDECD chromatogram of PCBs containing three–seven Cl-atoms/molecule. Column: DB-5ms, 30 m×0.25 mm I.D., d_f=0.25 μm, He at 50 cm/s, dopant gas 0.5% CH_4, detector flow-rate=45 ml/min, injector temperature=300°C, injector split ratio=40:1, 0.2 μl sample in methanol, 4.4 pg of each PCB. Oven temperature program: 80°C (1 min), 25°C/min to 190°C, 4°C/min to 240°C (2 min). PCB peaks: (1) 2,4,4′-trichlorobiphenyl, (2) 2,2′,5,5′-tetrachlorobiphenyl, (3) 2,2′,4,5,5′-pentachlorobiphenyl, (4) 2,3′,4,4′,5-pentachlorobiphenyl, (5) 2,2′,4,4′,5,5′-hexachlorobiphenyl, (6) 2,2′,3,4,4′,5′-hexachlorobiphenyl and (7) 2,2′,3,4,4′,5,5′-heptachlorobiphenyl.

there has been an interest in the analysis of inorganic elements, particularly metals, by the formation of relatively volatile compounds with organic constituents. Many references can be cited but the most comprehensive compilation of the earlier work is in a text by Moshier and Sievers [48]. Much of the emphasis in this area has been on the analysis of metals by the formation of volatile metal complexes. In general, these complexes are somewhat fragile and their decomposition is especially sensitive to metal surfaces and especially at high temperatures. In the early stages of gas chromatography, prior to the development of fused-silica capillary columns, avoiding exposure to metal surfaces presented a real challenge. PTFE columns packed with powdered PTFE were even used and they were not only inefficient but very difficult to make.

In order to attain a high sensitivity for the analysis, it was quickly recognized by Sievers and subsequent investigators that this was best accomplished using an ECD. Since the ECDs necessarily contained a radioactive foil, it was impossible to

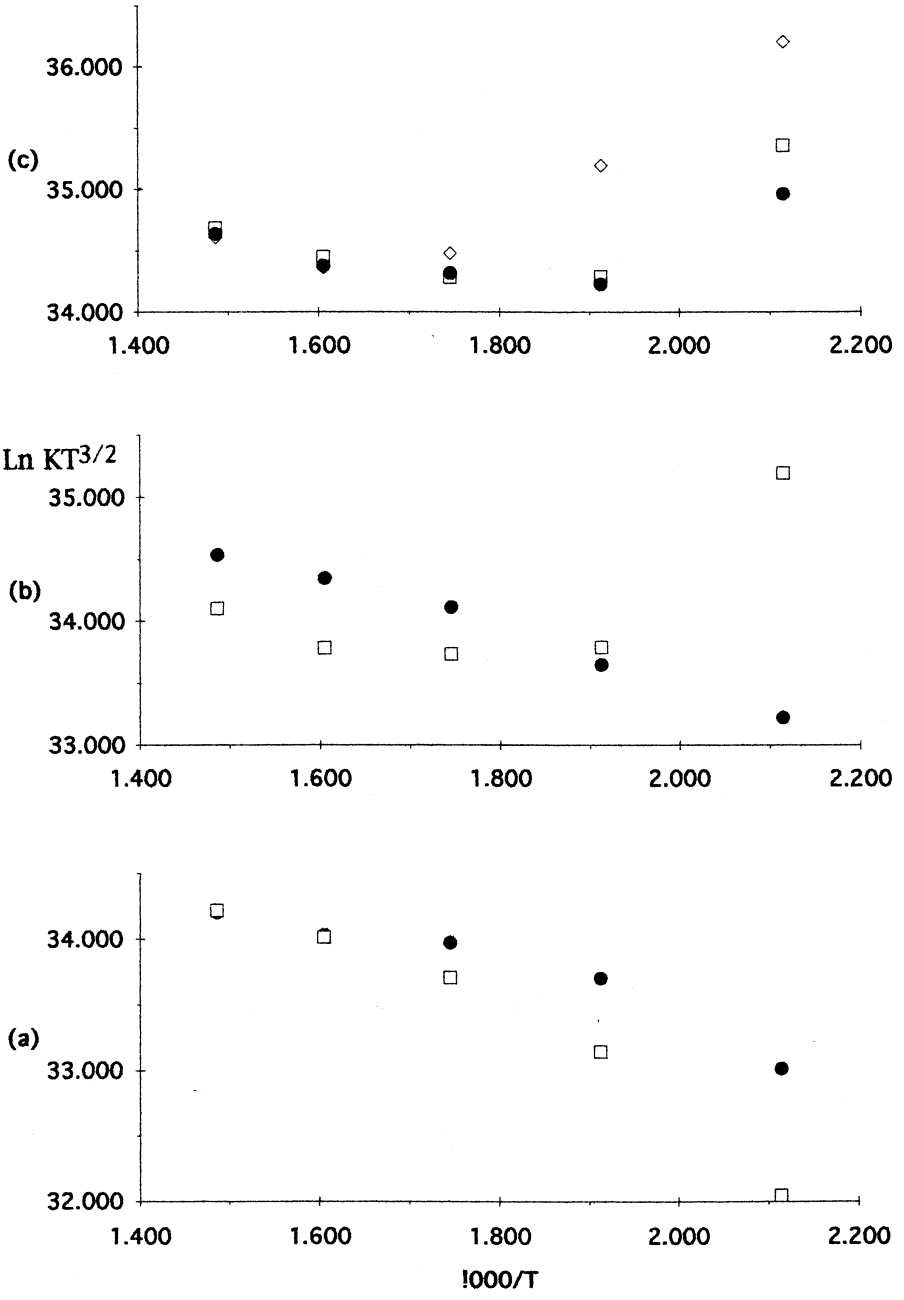

Fig. 14. Ln $KT^{3/2}$ versus $1/T$ for PCBs. (a) ● 2,4,4′-trichlorobiphenyl, □ 2,2′,5,5′-tetrachlorobiphenyl, (b) ● 2,2′,4,5,5′-pentachlorobiphenyl, □ 2,3′,4,4′,5-pentachlorobiphenyl, (c) ● 2,2′,4,4′,5,5′-hexachlorobiphenyl, □ 2,2,′,3,4,4′,5′-hexachlorobiphenyl, ◇ 2,2′,3,4,4′,5,5′-heptachlorobiphenyl.

avoid contact with this metal surface. Since the non-radioactive PDECD has essentially only a sapphire surface in the electron-capture region, it was thought that the PDECD would be especially advantageous for this analysis. Furthermore, the advanced development of fused-silica capillary columns that we enjoy today should also contribute heavily towards improving this type of analysis. This will not

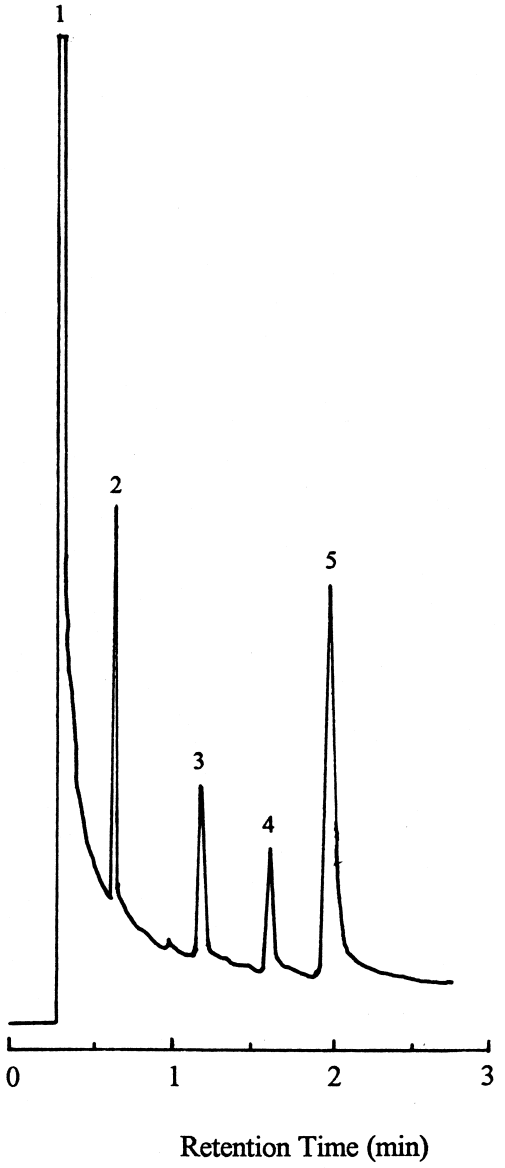

Fig. 15. Chromatogram using the PDECD for the analysis of metal–trifluoroacetylacetonates. (1) Solvent (toluene), (2) $Be(tfa)_2$ (0.4 pg), (3) $Al(tfa)_3$ (0.55 pg), (4) $Ga(tfa)_3$ (10 pg) and (5) $Cr(tfa)_3$ (0.42 pg). (tfa, trifluoroacetylacetonate).

only give more efficient separations but the use of small bore capillaries will speed up the analysis, shortening the residence time in the capillary column and minimizing decomposition in the heated column.

In our laboratory, we have considered several complexing agents for metal analysis but the ones that are most sensitive to electron capture are the trifluoroacetylacetonate complexes. The Be, Al and Cr complexes with trifluoroacetylacetone have unusual stability, are relatively volatile and have high electron-capture coefficients due to the highly electronegative fluorines. A relatively short narrow bore fused-silica capillary column (7 m×0.10 mm with 0.25 μm film thickness) was used for the analysis of these three metal complexes with the PDECD. The chromatogram is shown in Fig. 15 and the sharp peaks indicate little or no decomposition. The PDECD has remarkable sensitivity for these complexes, as shown in Table 6. The linearity of the PDECD response has also been evaluated and shown to be linear over at least three orders of magnitude. Graphs showing the linearity are given in Fig. 16.

Selenium reacts with 4-nitro-1,2-phenylene diamine to form 5-nitropiazselenol, which is relatively volatile and can be analyzed by GC. We have also used the PDECD for the detection of this selenium compound and found it to be reasonably sensitive. Since the compound does not have any highly electronegative groups, it will not have an exceptionally high electron-capture coefficient. However, it is sufficiently high to give an MDQ for selenium of 53 fg. This is far superior to other modes of detection. Again, the linearity of the response is over three orders of magnitude.

6. Use of the pulsed discharge electron-capture detector for liquid chromatography detection

A research program is presently underway to

Table 6
Minimum detectable quantity (MDQ) for metal trifluoroacetylacetonates using the PDECD

Metal complex	MDQ with PDECD	MDQ from literature	Ref.
$Be(trifloroacetylacetonate)_2$	1.2 fg	0.1 pg	[49]
$Cr(trifluoroaceylacetonate)_3$	3.6 fg	30. fg	[50]
$Al(trifluoroaceylacetonate)_3$	8.2 fg	80. fg	[51]

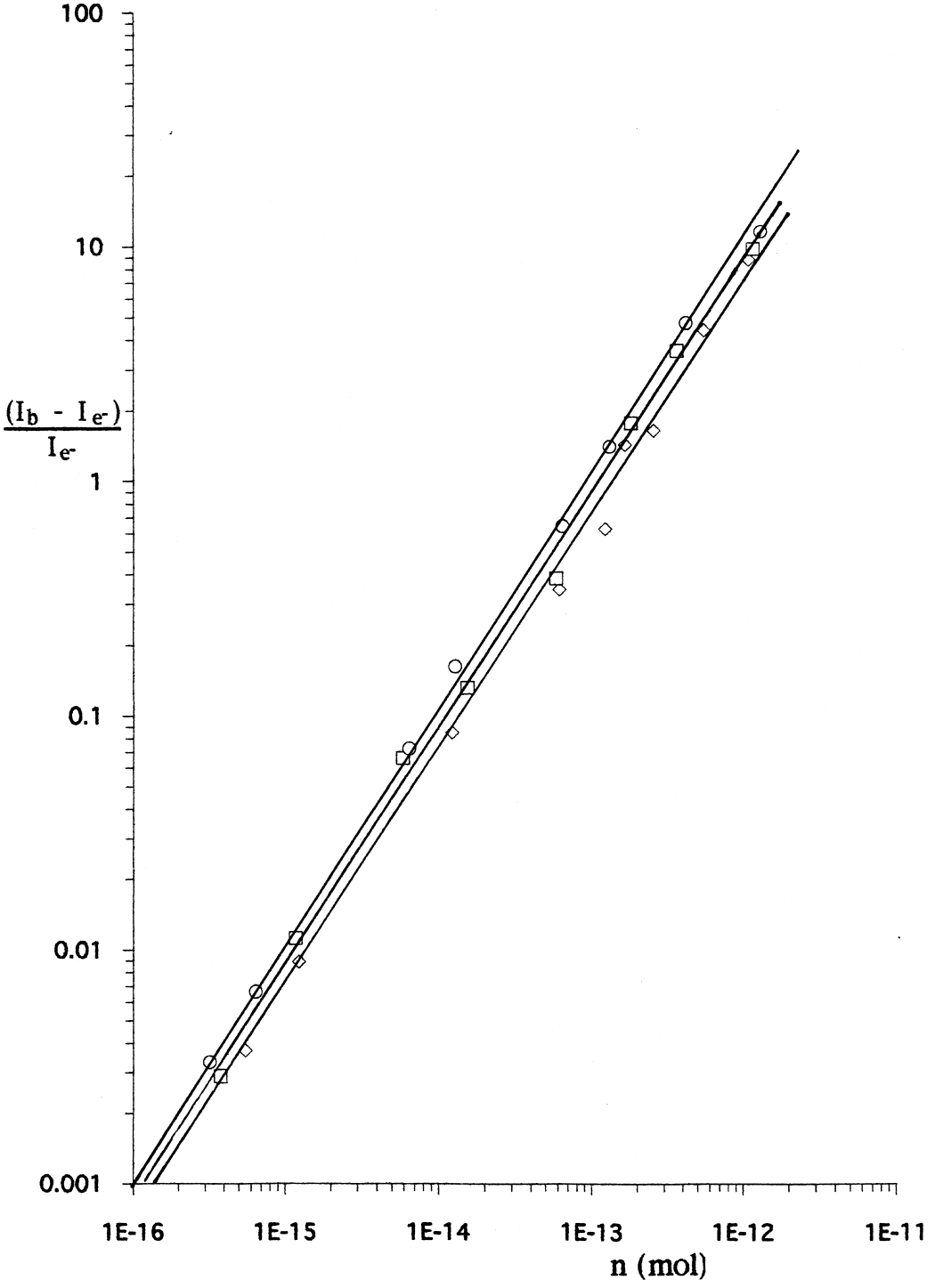

Fig. 16. Linearity of PDECD response for Be (○)–, Al(◇)– and Cr(□)–trifluoroacetylacetonates.

investigate the use of the PDECD as a detector for liquid chromatography (LC). In this project, we utilize the liquid carrier as the dopant in the PDECD. For this reason, it is imperative that the flow-rate and nature of the liquid phase are compatible with the operation of the PDECD. Typically, liquid flow-rates of 0.5–1.0 μl/min give a concentration of the dopant in the range of 0.2–1.0%. These concentrations are comparable to the concentration of methane normally used. The liquid carrier is nebulized prior to vaporization and this greatly assists in the vaporization process. Assuming that the liquid carrier is completely vaporized, it would serve as the dopant in the electron-capture process.

Preliminary results from this work have shown that saturated hydrocarbons such as isooctane and heptane serve in the role of dopant in very similar way to methane. In Table 1, we have listed several compounds that may be considered as possible dopants in the PDECD. The standing currents using isooctane and heptane are comparable and the electron-capture coefficients are essentially the same. Since the larger iso-octane and heptane should be very effective in the thermalization of the electrons, we would conclude that the smaller methane must be just as effective in this regard. On this basis, one would expect the saturated hydrocarbons intermediate in carbon number to also give comparable results. A brief study using propane as the dopant showed it to be comparable to methane.

If a higher-molecular-mass hydrocarbon were to be used as the dopant in the PDECD for GC analysis, it could be introduced through a permeation device. Careful control of temperature and flow-rate in the permeation apparatus would give good control of the concentration of dopant. One possible advantage of using higher-molecular-mass hydrocarbons is that their diffusion rate should be much less than that of methane and there would be less chance for diffusion into the discharge region. It is possible that a lower helium flow-rate could be used with the higher-molecular-mass hydrocarbons as dopants, and this would be most important for use of the PDECD in portable chromatographic units.

The study of using the PDECD as a detector for LC has also included polar liquid carriers that are used typically in LC analysis, such as acetonitrile and methanol and mixtures of these with water. Again, these liquids are serving as the dopant in the PDECD. Generally, the standing current is quite satisfactory with these liquids, but the electron capture is somewhat diminished compared to the use of saturated hydrocarbons. The reduction in electron capture is not so serious and the sensitivity of the PDECD is still superior to that of other detectors commonly used in LC work. The sensitivity and linearity using these polar liquids is currently under investigation and will be reported at a later date.

The use of the radioactive ECD as a detector for LC has been investigated since almost the inception of the electron-capture detector. Since the β-particles from the radioactive foil are so energetic, they can ionize the inert carrier gas and the role of the dopant is quite different from that in the PDECD. It is probable that the radioactive ECD would be more forgiving with regards to the presence of polar compounds. On the other hand, the inertness of the PDECD may play an important role in its use as a LC detector, whereas the radioactive ECD may be prone to contamination in the presence of the higher-molecular-mass compounds.

7. Conclusions

The following are the essential features of the non-radioactive PDECD:

1. Using methane as the dopant, the PDECD behaves similarly to the radioactive ECD. The relative responses from the PDECD are equal to or greater than those from the conventional radioactive ECD.
2. Due to the inertness of the sapphire walls within the PDECD, there is less adsorption compared to metallic surfaces. This allows electron-capture measurements at lower temperatures. This is especially important in analyses involving thermally unstable compounds such as pesticides and metal complexes.
3. The PDECD response is linear over four orders of magnitude in the constant potential mode for compounds that have good chromatographic behavior. This can be extended in the constant current mode to five orders of magnitude.
4. The sensitivity of the PDECD is equal to or better than that of the radioactive ECD.

5. The internal volume of the detector is ~55 μl, which gives a residence time of 0.08 s when the discharge gas flow-rate is 40 ml/min. This allows the PDECD to be used in high-speed chromatography.
6. Elimination of the radioactive foil eliminates the need for radioactive leak tests and allows the GC–PDECD system to be transferred to another location without any restrictions.

Acknowledgements

The authors would like to thank The Robert A. Welch Foundation for financial support of this work in Grant E-059. Also, this work could not have been performed without the support of Valco Insruments Co., Inc. in the form of funding of Graduate Students stipends, spectroscopic equipment, critical gas chromatographic supplies, and machine work and technical assistance in detector design.

References

[1] W.E. Wentworth, S.D. Stearns, US Pat., 5 153 519 (1992).
[2] W.E. Wentworth, S.D. Stearns, US Pat., 5 317 271 (1994).
[3] W.E. Wentworth, S.D. Stearns, US Pat., 5 394 090 (1995).
[4] W.E. Wentworth, S.D. Stearns, US Pat., 5 394 091 (1995).
[5] W.E. Wentworth, S.D. Stearns, US Pat., 5 394 092 (1995).
[6] W.E. Wentworth, S.D. Stearns, US Pat., 5 528 150 (1996).
[7] W.E. Wentworth and S.D. Stearns, US Pat., 5 532 599 (1996).
[8] W.E. Wentworth and S.D. Stearns, US Pat., 5 541 519 (1996).
[9] W.E. Wentworth and S.D. Stearns, US Pat., 5 594 346 (1997).
[10] J.E. Lovelock, S.R. Lipsky, J. Am. Chem. Soc. 82 (1960) 431.
[11] J.E. Lovelock, N.L. Gregory, in: N. Brenner (Ed.), Gas Chromatography, Academic Press, New York, 1962, p. 219.
[12] R.J. Maggs, P.L. Joynes, A.J. Davies, J.E. Lovelock, Anal. Chem. 43 (1971) 1966.
[13] CRC Handbook of Chemistry and Physics, 74th ed, CRC Press, Boca Raton, FL, 1993–1994.
[14] W.E. Wentworth, E. Chen, J.E. Lovelock, J. Phys. Chem. 70 (1966) 445.
[15] J.H. Bochinski, J.C. Sternberg, in: Abstracts for the 148th National Meeting of the American Chemical Society, 1964, p. Abstract52,22A.
[16] W.E. Wentworth, T. Limero, C.F. Batten, E.C.M. Chen, J. Chromatogr. 441 (1988) 45.
[17] W.E. Wentworth, T. Limero, C.F. Batten, E.C.M. Chen, J. Chromatogr. 468 (1989) 215.
[18] A. Neukermans, W. Kruger, D. McManigill, J. Chromatogr. 259 (1983) 1.
[19] P.G. Simmonds, J. Chromatogr. 399 (1987) 149.
[20] W.E. Wentworth, E.D. D'Sa, H. Cai, S.D. Stearns, J. Chromatogr. Sci. 20 (1992) 478.
[21] W.E. Wentworth, S. Wiedeman, Y. Qin, J. Madabushi, S.D. Stearns, J. Applied Spectrosc. 49 (1995) 1282.
[22] W.E. Wentworth, S.V. Vasnin, S.D. Stearns, C.J. Meyer, Chromatographia 34 (1992) 219.
[23] W.E. Wentworth, H. Cai, S.D. Stearns, J. Chromatogr. A 688 (1994) 135.
[24] G. Gremaud, W.E. Wentworth, A. Zlatkis, R. Swatloski, E.C.M. Chen, S.D. Stearns, J. Chromatogr. A 724 (1996) 235.
[25] W.E. Wentworth, Y. Li, S.D. Stearns, J. High Resolut. Chromatogr. 19 (1996) 95.
[26] W.E. Wentworth, N. Helias, A. Zlatkis, E.C.M. Chen, S.D. Stearns, J. Chromatogr. A 745 (1998) 319.
[27] W.E. Wentworth, A. Tishbee, C.F. Batten, A. Zlatkis, J. Chromatogr. 112 (1975) 229.
[28] S. Kapila, D.J. Bornhop, S.E. Manahan, G.L. Nickel, J. Chromatogr. 259 (1983) 205.
[29] W.E. Wentworth, E.C.M. Chen, in: A. Zlatkis, C.F. Poole (Eds.), Electron Capture—Theory and Practice in Chromatography, Journal of Chromatography Library, Vol. 20, Elsevier, Amsterdam, 1981, p. 27, Ch. 3.
[30] E.C.M. Chen, W.E. Wentworth, E.D. D'Sa, C.F. Batten, J. Chromatogr. 399 (1987) 121.
[31] W.E. Wentworth, Y. Wang, W. Odegard, E.C.M. Chen, S.D. Stearns, J. Chromatogr. Sci. 34 (1996) 368.
[32] H. Cai, W.E. Wentworth, S.D. Stearns, Anal. Chem. 68 (1996) 1233.
[33] J. Huang, M.Sc. Thesis, 1996.
[34] E.C.M. Chen, personal communication.
[35] H. Cai, S.D. Stearns, W.E. Wentworth, Anal. Chem. 70 (1998) 3770.
[36] W.E. Wentworth, J.C. Steelhammer, in: E.J. Hart (Ed.), Radiation Chemistry, Advances in Chemistry Series, American Chemical Society, Washington, DC, 1968, p. 75, Ch. 4.
[37] W.E. Wentworth, E.C.M. Chen, J. Chromatogr. 186 (1979) 99.
[38] E.D. D'sa, W.E. Wentworth, E.C.M. Chen, J. Phys. Chem. 92 (1988) 285.
[39] E.C.M. Chen, W.E. Wentworth, E. Desai, C.F. Batten, J. Chromatogr. 399 (1987) 121.
[40] W.E. Wentworth, R.S. Becker, R. Tung, J. Phys. Chem. 71 (1967) 1652.
[41] E.C.M. Chen, R. George, S. Carr, W.E. Wentworth, E.S.D. Chen, J. Chromatogr. A 811 (1998) 250.
[42] W.B. Knighton, J.A. Bognar, E.P. Grimsrud, J. Mass Spectrom. 30 (1995) 557.
[43] E.P. Grimsrud, S. Chowdury, P. Kebarle, J. Chem. Phys. 83 (1995) 3983.
[44] E.C.M. Chen, W.E. Wentworth, Mol. Cryst. Liq. Cryst. 171 (1987) 271.

[45] A. Nakajima, T. Naguwa, K. Knakao, K. Hoshino, T. Sugioka, T. Naganuma, F. Ono, K. Watanabe, K. Knakao, Y. Konishi, R. Kishi, K. Kaya, Chem. Phys. Lett. 96 (1993) 2385.
[46] W.E. Wentworth, J. Huang, E.C.M. Chen, S.D. Stearns, Chromatographia 43 (1996) 353.
[47] G.P. Jackson, A. Andrewes, Analyst 123 (1998) 1085.
[48] R.W. Moshier, R.E. Sievers, Gas Chromatography of Metal Chelates, Pergamon Press, Oxford, 1965.
[49] T.A. Gosink, Anal. Chem. 47 (1975) 165.
[50] J. Savory, P. Mushak, F.W. Sunderman, R.H. Estes, N.O. Roszel, Anal. Chem. 42 (1971) 165.
[51] M.L. Taylor, E.L. Arnold, Anal. Chem. 43 (1971) 1328.